9012 *Inorg. Chem.* **2010**, *49*, 9012–9025
DOI: 10.1021/ic101445n

Inorganic Chemistry
Article

Syntheses, Structures, and Magnetic Properties of Diphenoxo-Bridged $Cu^{II}Ln^{III}$ and Ni^{II}(Low-Spin)Ln^{III} Compounds Derived from a Compartmental Ligand (Ln = Ce−Yb)

Arpita Jana,[†] Samit Majumder,[†] Luca Carrella,[‡] Malabika Nayak,[†] Thomas Weyhermueller,[§] Supriya Dutta,[∥] Dieter Schollmeyer,[⊥] Eva Rentschler,*[,‡] Rajesh Koner,*[,†] and Sasankasekhar Mohanta*[,†]

[†]*Department of Chemistry, University of Calcutta, 92 A. P. C. Road, Kolkata 700 009, India,* [‡]*Institut für Anorganische Chemie und Analytische Chemie, Johannes-Gutenberg, Universität Mainz, Duesbergweg 10-14, D-55128 Mainz, Germany,* [§]*Max-Planck-Institut für Bioanorganische Chemie, Stiftstrasse 34-36, D-45470 Mülheim an der Ruhr, Germany,* [∥]*Department of Inorganic Chemistry, Indian Association for Cultivation of Science, India, and* [⊥]*Institut für Organische Chemie, Universität Mainz, Duesbergweg 10-14 55099 Mainz, Germany*

Received July 20, 2010

Syntheses, characterization, and magnetic properties of a series of diphenoxo-bridged discrete dinuclear $M^{II}Ln^{III}$ complexes (M = Cu or Ni, Ln = Ce−Yb) derived from the compartmental Schiff base ligand, H_2L, obtained on condensation of 3-ethoxysalicylaldehyde with *trans*-1,2-diaminocyclohexane, are described. Single crystal X-ray structures of eight $Cu^{II}Ln^{III}$ compounds (Ln = Ce (**1**), Pr (**2**), Nd (**3**), Sm (**4**), Tb (**7**), Ho (**9**), Er (**10**), and Yb (**12**)) and three $Ni^{II}Ln^{III}$ (Ln = Ce (**13**), Sm (**16**), and Gd (**18**)) compounds have been determined. Considering the previously reported structure of the $Cu^{II}Gd^{III}$ (**6**) compound (*Eur. J. Inorg. Chem.* **2005**, 1500), a total of twelve structures are discussed/compared in this study. Four types of composition are observed in the $Cu^{II}Ln^{III}$ complexes: $[Cu^{II}LLn^{III}(NO_3)_3(H_2O)]$ (**1**−**3**: Ln = Ce−Nd), $[Cu^{II}LSm^{III}(NO_3)_3]\cdot CH_3COCH_3$ (**4**), $[Cu^{II}(H_2O)LLn^{III}(NO_3)_3]$ (**5**: Ln = Eu; **6**: Ln = Gd), and $[Cu^{II}LLn^{III}(NO_3)_3]$ (**4A**: Ln = Sm; **7**−**12**: Ln = Tb−Yb). On the other hand, the $Ni^{II}Ln^{III}$ complexes are characterized to have two types of composition: $[Ni^{II}LLn^{III}(H_2O)(NO_3)_3]$ (**13**−**15**: Ln = Ce−Nd) and $[Ni^{II}LLn^{III}(NO_3)_3]\cdot 0.5CH_3COCH_3$ (**16**−**24**: Ln = Sm−Yb). Among twelve X-ray structures, seven belong to three different isomorphous sets ($Cu^{II}Ce^{III}$ (**1**), $Cu^{II}Pr^{III}$ (**2**), $Cu^{II}Nd^{III}$ (**3**), and $Ni^{II}Ce^{III}$ (**13**); $Cu^{II}Tb^{III}$ (**7**), $Cu^{II}Ho^{III}$ (**9**), $Cu^{II}Er^{III}$ (**10**), and $Cu^{II}Yb^{III}$ (**12**); $Ni^{II}Sm^{III}$ (**16**) and $Ni^{II}Gd^{III}$ (**18**)), whereas space group/unit cell parameters of two others ($Cu^{II}Sm^{III}$ (**4**) and $Cu^{II}Gd^{III}$ (**6**)) are of different types. The lanthanide(III) centers in $Cu^{II}Ce^{III}$ (**1**), $Cu^{II}Pr^{III}$ (**2**), $Cu^{II}Nd^{III}$ (**3**), and $Ni^{II}Ce^{III}$ (**13**) complexes are eleven-coordinated, while the lanthanide(III) centers in other compounds are ten-coordinated. As evidenced from the dihedral angle (δ) between the $CuO(phenoxo)_2$ and $LnO(phenoxo)_2$ planes, variation in the extent of planarity of the bridging moiety in the $Cu^{II}Ln^{III}$ compounds takes place; the ranges of δ values are 0.8−6.2° in the $4f^{1-7}$ analogues and 17.6−19.1° in the $4f^{8-13}$ analogues. The $Cu^{II}Gd^{III}$ (**6**) compound exhibits ferromagnetic interaction (*Eur. J. Inorg. Chem.* **2005**, 1500). The nature of the magnetic exchange interaction in the $Cu^{II}Ln^{III}$ complexes has been understood by utilizing the empirical approach; the $Ni^{II}Ln^{III}$ complexes have been used as references. The metal centers in the Eu^{III} complex are uncorrelated, while other $4f^{1-6}$ analogues (Ce^{III}, Pr^{III}, Nd^{III}, and Sm^{III}) exhibit antiferromagnetic interaction. Among the higher analogues ($4f^{7-13}$), only Yb^{III} exhibits antiferromagnetic interaction, while interaction in other analogues (Gd^{III}, Tb^{III}, Dy^{III}, Ho^{III}, Er^{III}, and Tm^{III}) is ferromagnetic. An important aspect of the present study is the measurement of the magnetic susceptibility of the unblocked samples as well as on blocking the samples with grease to avoid powder reorientation, if any. Comparison of the two sets of data reveals significant difference in some cases.

Introduction

Molecular magnetism has been a frontier research area.[1−17] During the past few decades, many studies have been carried out to understand the intimate relationship of spin coupling and to utilize the derived ideas to develop molecule-based magnetic materials.[1−16] However, in comparison to the extensive studies on 3d−3d systems,[1−4] magnetic properties of 3d−4f complexes or other types of systems containing lanthanides as one spin carrier have been much less investigated.[1a,3a,5−17]

*To whom correspondence should be addressed. E-mail: sm_cu_chem@yahoo.co.in (S.M.), rentschl@uni-mainz.de (E.R.), rk_cu_chem@yahoo.co.in (R.K.).

 Published on Web 09/02/2010

Among the trivalent lanthanide ions, only gadolinium(III) is isotropic, and therefore the understanding of the nature of the exchange interaction and the evaluation of the value of exchange integral in Gd^{III} containing complexes are similar to those in 3d−3d systems.[5−10] In contrast, even the understanding of the nature of the interaction is complicated for the systems containing other lanthanides, which are anisotropic and exhibit temperature dependence Stark level population variance.[11−17] The problem can be overcome by an empirical approach in which the $\chi_M T$ of a reference compound is subtracted from that of the exchange coupled compound, having the same lanthanide in a diamagnetic environment.[11−15] A conclusion about the ferromagnetic and antiferromagnetic nature can then be made if the difference, $\Delta\chi_M T$, between the $\chi_M T$'s of the exchange-coupled and reference compound increases and decreases, respectively, on lowering of temperature.[11−15] However, as both the exchange-coupled and reference compound should have similar structures or at least similar coordination environment for the 4f metal ion, the utilization of the empirical approach is not an easy task. Previously, the nature of the interaction in a few series has been understood by the empirical approach.[11−15] However, the results are not in line with each other or fully with the theoretical proposition.[11]

Chart 1. Chemical Structures of H_2L, H_2L^1, and H_2L^2

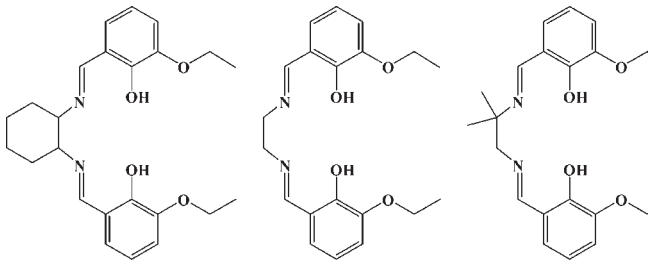

The extent of ferromagnetic interaction in diphenoxo-bridged $Cu^{II}Gd^{III}$ complexes increases, as theoretically predicted,[6] with the decrease of the dihedral angle (δ) between the $CuO(phenoxo)_2$ and $GdO(phenoxo)_2$ planes.[5−8,10] For example, the J values of the $Cu^{II}Gd^{III}$ complexes derived from H_2L, H_2L^1, and H_2L^2 (Chart 1), having δ values 2.1, 4.3, and 12.9°, are 6.3, 4.04, and 3.5 cm^{-1}, respectively.[8a,14,15] The nature of interaction and the qualitative understanding of the strength of interaction of the full series of $Cu^{II}Ln^{III}$ complexes derived from H_2L^1 and H_2L^2 have also been investigated.[14,15] The extent of interaction between copper(II) and lanthanide(III) in the systems derived from H_2L^2 is weak,[14] as expected because of the participation of deep-seated 4f orbitals in exchange coupling. In fact, only weak interaction is observed in most of the systems containing a 4f metal ion as one spin carrier.[5−14,16] In contrast, surprisingly strong exchange interaction has been observed in some of the $Cu^{II}Ln^{III}$ complexes derived from H_2L^1.[15] As the δ value (ca. 4°) in the $Cu^{II}Ln^{III}$ complexes derived from H_2L^1 is less than that in the $Cu^{II}Ln^{III}$ complexes derived from H_2L^2 (ca. 13.5°), it seems that strong exchange interaction in the former series is related to their more planar $CuO(phenoxo)_2Ln$ bridging core.[15] As already mentioned, the δ value (2.1°) in the $Cu^{II}Gd^{III}$ complex, derived from H_2L, is approximately half of the δ value (4.3°) in the $Cu^{II}Gd^{III}$ complex derived

(1) (a) Kahn, O. *Molecular Magnetism*; VCH Publications: New York, 1993. (b) *Magneto-Structural Correlations in Exchange Coupled Systems*; Willet, R. D., Gatteschi, D., Kahn, O., Eds.; D. Reidel: Dordrecht, The Netherlands, 1985. (c) *Research Frontiers in Magnetochemistry*; O'Connor, C. J., Ed.; World Scientific: Singapore, 1993.

(2) (a) Niemann, A.; Bossek, U.; Wieghardt, K.; Butzlaff, C.; Trautwein, A. X.; Nuber, B. *Angew. Chem., Int. Ed. Engl.* **1992**, *31*, 311–313. (b) Nanda, K. K.; Thompson, L. K.; Bridson, J. N.; Nag, K. *J. Chem. Soc., Chem. Commun.* **1994**, 1337–1338. (c) Chou, Y.-C.; Huang, S.-F.; Koner, R.; Lee, G.-H.; Wang, Y.; Mohanta, S.; Wei, H.-H. *Inorg. Chem.* **2004**, *43*, 2759–2761. (d) Koner, R.; Hazra, S.; Fleck, M.; Jana, A.; Lucas, C. R.; Mohanta, S. *Eur. J. Inorg. Chem.* **2009**, 4982–4988. (e) Paine, T. K.; Rentschler, E.; Weyhermüller, T.; Chaudhuri, P. *Eur. J. Inorg. Chem.* **2003**, 3167–3178.

(3) (a) *Single-Molecule Magnets and Related Phenomena*; Winpenny, R., Ed.; Springer: New York, 2006. (b) *Extended Linear Chain Compounds*; Miller, J. S., Ed.; Plenum: New York, 1983; Vol. *III*. (c) *Magnetic Molecular Materials*; Gatteschi, D., Kahn, O., Miller, J. S., Palacio, F., Eds.; Kluwer Academic Publishers: Dordrecht, The Netherlands, 1991. (d) *Magnetism: Molecules to Materials II*; Miller, J. S., Drillon, M., Eds.; Wiley-VCH: Weinheim, 2001.

(4) (a) Ribas, J.; Escuer, A.; Monfort, M.; Vicente, R.; Cortés, R.; Lezama, L.; Rojo, T. *Coord. Chem. Rev.* **1999**, *193*−*195*, 1027–1068. (b) Verdaguer, M.; Bleuzen, A.; Marvaud, V.; Vaissermann, J.; Seuleiman, M.; Desplanches, C.; Scuiller, A.; Train, C.; Garde, R.; Galley, G.; Lomenech, C.; Rosenman, I.; Veillet, P.; Cartier, C.; Villain, F. *Coord. Chem. Rev.* **1999**, *190*−*192*, 1023–1047. (c) Stamatatos, T. C.; Foguet-Albiol, D.; Lee, S.-C.; Stoumpos, C. C.; Raptopoulou, C. P.; Terzis, A.; Wernsdorfer, W.; Hill, S. O.; Perlepes, S. P.; Christou, G. *J. Am. Chem. Soc.* **2007**, *129*, 9484–9499.

(5) (a) Winpenny, R. E. P. *Chem. Soc. Rev.* **1998**, 447–452. (b) Sakamoto, M.; Manseki, K.; Ōkawa, H. *Coord. Chem. Rev.* **2001**, *219*−*221*, 379–414. (c) Bencini, A.; Benelli, C.; Caneschi, A.; Carlin, R. L.; Dei, A.; Gatteschi, D. *J. Am. Chem. Soc.* **1985**, *107*, 8128–8136. (d) Sasaki, M.; Manseki, K.; Horiuchi, H.; Kumagai, M.; Sakamoto, M.; Nishida, H.; Sakiyama, Y.; Sakai, M.; Sadaoka, Y.; Ohba, M.; Ōkawa, H. *J. Chem. Soc., Dalton Trans.* **2000**, 259–263. (e) Benelli, C.; Murrie, M.; Parson, S.; Winpenny, R. E. P. *J. Chem. Soc., Dalton Trans.* **1999**, 4125–4126.

(6) Ramade, I.; Kahn, O.; Jeannin, Y.; Robert, F. *Inorg. Chem.* **1997**, *36*, 930–936.

(7) Costes, J.-P.; Dahan, F.; Dupuis, A. *Inorg. Chem.* **2000**, *39*, 165–168.

(8) (a) Koner, R.; Lee, G.-H.; Wang, Y.; Wei, H.-H.; Mohanta, S. *Eur. J. Inorg. Chem.* **2005**, 1500–1505. (b) Mohanta, S.; Lin, H.-H.; Lee, C.-J.; Wei, H.-H. *Inorg. Chem. Commun.* **2002**, *5*, 585–588.

(9) (a) Costes, J.-P.; Dahan, F.; Dupuis, A.; Laurent, J.-P. *Inorg. Chem.* **2000**, *39*, 169–173. (b) Costes, J.-P.; Dahan, F.; Donnadieu, B.; Garcia-Tojal, J.; Laurent, J.-P. *Eur. J. Inorg. Chem.* **2001**, 363–365.

(10) (a) Costes, J.-P.; Dahan, F.; Dupuis, A.; Laurent, J.-P. *Inorg. Chem.* **1996**, *35*, 2400–2402. (b) Costes, J.-P.; Dahan, F.; Dupuis, A.; Laurent, J.-P. *Inorg. Chem.* **1997**, *36*, 3429–3433. (c) Costes, J.-P.; Dahan, F.; Dupuis, A.; Laurent, J.-P. *Inorg. Chem.* **1997**, *36*, 4284–4286. (d) Novitchi, G.; Shova, S.; Caneschi, A.; Costes, J.-P.; Gdaniec, M.; Stanica, N. *Dalton Trans.* **2004**, 1194–1200. (e) Costes, J.-P.; Dahan, F.; Novitchi, G.; Arion, V.; Shova, S.; Lipkowski, J. *Eur. J. Inorg. Chem.* **2004**, 1530–1537.

(11) Kahn, M. L.; Mathonière, C.; Kahn, O. *Inorg. Chem.* **1999**, *38*, 3692–3697.

(12) Kahn, M. L.; Sutter, J.-P.; Golhen, S.; Guionneau, P.; Ouahab, L.; Kahn, O.; Chasseau, D. *J. Am. Chem. Soc.* **2000**, *122*, 3413–3421.

(13) Figuerola, A.; Diaz, C.; Ribas, J.; Tangoulis, V.; Granell, J.; Lloret, F.; Mahia, J.; Maestro, M. *Inorg. Chem.* **2003**, *42*, 641–649.

(14) Costes, J.-P.; Dupuis, A.; Laurent, J.-P. *Chem.—Eur. J.* **1998**, 1616–1620.

(15) Koner, R.; Lin, H.-H.; Wei, H.-H.; Mohanta, S. *Inorg. Chem.* **2005**, *44*, 3524–3526.

(16) (a) Westin, L. G.; Kritikos, M.; Caneschi, A. *Chem. Commun.* **2003**, 1012–1013. (b) Brechin, E. K.; Harris, S. G.; Parson, S.; Winpenny, R. E. P. *J. Chem. Soc., Dalton Trans.* **1997**, 1665–1666. (c) Sanz, J. L.; Ruiz, R.; Gleizes, A.; Lloret, F.; Faus, J.; Julve, M.; Borrás-Almenar, J.; Journaux, Y. *Inorg. Chem.* **1996**, *35*, 7384–7393. (d) Chen, Q.-H.; Luo, Q.-H.; Wang, Z.-L.; Chen, J.-T. *Chem. Commun.* **2000**, 1033–1034.

(17) (a) Kyatskaya, S.; Mascarós, J. R. G.; Bogani, L.; Hennrich, F.; Kappes, M.; Wernsdorfer, W.; Ruben, M. *J. Am. Chem. Soc.* **2009**, *131*, 15143–15151. (b) Branzoli, F.; Carretta, P.; Filibian, M.; Zoppellaro, G.; Graf, M. J.; Galan-Mascaros, J. R.; Fuhr, O.; Brink, S.; Ruben, R. *J. Am. Chem. Soc.* **2009**, *131*, 4387–4396. (c) Ishikawa, N.; Sugita, M.; Ishikawa, T.; Koshihara, S.; Kaizu, Y. *J. Am. Chem. Soc.* **2003**, *125*, 8694–8695. (d) Bian, Y.; Jiang, J.; Tao, Y.; Choi, M. T. M.; Li, R.; Ng, A. C. H.; Zhu, Z-Y; Li, H.-W.; Mak, T. C. W.; Ng, D. K. P. *J. Am. Chem. Soc.* **2003**, *125*, 12257–12276. (e) Ishikawa, N.; Sugita, M.; Tanaka, N.; Ishikawa, T.; Koshihara, S.; Kaizu, Y. *Inorg. Chem.* **2004**, *43*, 5498–5500.

Table 1. Crystallographic Data for the Eight $Cu^{II}Ln^{III}$ Complexes (**1**−**4**, **7**, **9**, **10**, and **12**)

	$Cu^{II}Ce^{III}$ (**1**)	$Cu^{II}Pr^{III}$ (**2**)	$Cu^{II}Nd^{III}$ (**3**)	$Cu^{II}Sm^{III}$ (**4**)	$Cu^{II}Tb^{III}$ (**7**)	$Cu^{II}Ho^{III}$ (**9**)	$Cu^{II}Er^{III}$ (**10**)	$Cu^{II}Yb^{III}$ (**12**)
empirical formula	$C_{24}H_{30}N_5O_{14}CuCe$	$C_{24}H_{21}N_5O_{14}CuPr$	$C_{24}H_{26}N_5O_{14}CuNd$	$C_{27}H_{34}N_5O_{14}CuSm$	$C_{24}H_{28}N_5O_{13}CuTb$	$C_{24}H_{28}N_5O_{13}CuHo$	$C_{24}H_{28}N_5O_{13}CuEr$	$C_{24}H_{28}N_5O_{13}CuYb$
fw	816.19	807.91	816.28	866.48	816.97	822.98	825.31	831.1
crystal color	red	red	red	red	red	red	red	red
crystal system	monoclinic	monoclinic	monoclinic	monoclinic	monoclinic	monoclinic	monoclinic	monoclinic
space group	$P2_1/c$	$P2_1/c$	$P2_1/c$	$P2_1/c$	$P2_1/n$	$P2_1/n$	$P2_1/n$	$P2_1/n$
a (Å)	14.4630(15)	14.5748(6)	14.5049(12)	8.9667(7)	8.5332(10)	8.5253(4)	8.5644(5)	8.5876(3)
b (Å)	14.0961(15)	14.1728(6)	14.1215(12)	18.1816(14)	25.402(3)	25.223(2)	25.4504(12)	25.2526(9)
c (Å)	15.6604(16)	15.7861(7)	15.6703(13)	21.9041(15)	13.281(2)	13.2679(7)	13.1553(7)	13.2704(5)
α (deg.)	90.00	90.00	90.00	90.00	90.00	90.00	90.00	90.00
β (deg.)	117.306(2)	116.896(2)	116.969(2)	110.655(3)	101.029(3)	101.428(4)	100.185(3)	100.290(2)
γ (deg.)	90.00	90.00	90.00	90.00	90.00	90.00	90.00	90.00
V (Å^3)	2836.9(5)	2908.1(2)	2860.7(4)	3341.5(4)	2825.6(6)	2796.5(3)	2822.2(3)	2831.52(18)
Z	4	4	4	4	4	4	4	4
T, K	100(2)	296(2)	120(2)	296(2)	100(2)	100(2)	193(2)	193(2)
2θ (deg.)	3.16−75.0	4.08−61.50	3.16−51.34	3.0−51.14	6.42−65.00	5.84−65.00	4.48−56.00	5.08−56.54
μ (mm^{-1})	2.415	2.465	2.618	2.450	3.312	3.647	3.783	4.110
ρ_{calcd} (g cm^{-3})	1.911	1.845	1.895	1.722	1.920	1.955	1.942	1.950
F(000)	1632	1600	1624	1736	1620	1628	1632	1640
absorption correction	multi-scan	multi-scan	multi-scan	multi-scan	multi-scan	multi-scan	empirical	empirical
index ranges	$-24 \le h \le 24$	$-20 \le h \le 20$	$-17 \le h \le 17$	$-10 \le h \le 10$	$-12 \le h \le 12$	$-12 \le h \le 12$	$-10 \le h \le 11$	$-11 \le h \le 10$
	$-24 \le k \le 24$	$-20 \le k \le 20$	$-17 \le k \le 17$	$-22 \le k \le 21$	$-38 \le k \le 38$	$-38 \le k \le 38$	$-27 \le k \le 33$	$-31 \le k \le 33$
	$-26 \le l \le 26$	$-22 \le l \le 22$	$-19 \le l \le 19$	$-26 \le l \le 26$	$-20 \le l \le 20$	$-20 \le l \le 20$	$-17 \le l \le 16$	$-17 \le l \le 17$
reflections collected	211645	55083	34391	40483	86504	66912	24579	28494
independent reflections (R_{int})	14903(0.0333)	9045(0.0570)	5418(0.1018)	6246(0.0548)	10212(0.0367)	10087(0.0435)	6411(0.1145)	7009(0.1030)
R_1[a]/ wR_2[b] ($I > 2\sigma(I)$)	0.0242/0.0592	0.0349/0.1081	0.0520/0.1368	0.0418/0.0999	0.0627/0.1417	0.0390/0.0882	0.0541/0.0930	0.0399/0.0800
R_1[a]/ wR_2[b] (for all data)	0.0286/0.0614	0.0544/0.1252	0.0795/0.1563	0.0630/0.1120	0.0654/0.1429	0.0497/0.0935	0.1126/0.1088	0.0776/0.0885

[a] $R_1 = [\sum||F_o| - |F_c||/\sum|F_o|]$. [b] $wR_2 = [\sum w(F_o^2 - F_c^2)^2/\sum wF_o^4]^{1/2}$.

from H_2L[1].[8a] We therefore anticipated that the $Cu^{II}Ln^{III}$ complexes derived from H_2L should exhibit very strong exchange interaction. With this aim to get strongly coupled 3d−4f systems, we report herein the syntheses, characterization, structures, and variable-temperature (2−300 K) magnetic properties of the full series of $M^{II}Ln^{III}$ complexes (M = Cu or low-spin Ni, Ln = Ce−Yb) derived from H_2L.

Experimental Section

Materials and Physical Measurements. All the reagents and solvents were purchased from the commercial sources and used as received. The Schiff base ligand (H_2L) has been synthesized by the condensation of 3-ethoxysalicyldehyde with *trans*-1,2-diaminocyclohexane. $[Cu^{II}L\subset(H_2O)]$ was prepared according to the reported method.[8a] $[Ni^{II}L\subset(H_2O)]$ was prepared following the procedure, similar to that of $[Cu^{II}L\subset(H_2O)]$. Elemental (C, H, and N) analyses were performed on a Perkin-Elmer 2400 II analyzer. IR spectra were recorded in the region 400−4000 cm^{-1} on a Bruker-Optics Alpha-T spectrophotometer with samples as KBr disks. Variable-temperature (2−300 K) magnetic susceptibility measurements were carried out with a Quantum Design MPMS SQUID magnetometer. Diamagnetic corrections were estimated from the Pascal constants. Magnetic susceptibility data of all the unblocked samples were collected at 1 T field strength. In these data for some samples powder reorientations were guessed. To check and to omit the powder reorientation effect the data for these samples were recollected at 1 T with powders blocked with grease. Diamagnetic correction of the grease was measured separately and considered in the calculation of the susceptibility of the blocked samples.

Syntheses of $[M^{II}LLn^{III}(NO_3)_3(H_2O)]$ (1−3: M = Cu, Ln = Ce−Nd; 13−15: M = Ni, Ln = Ce−Nd), $[Cu^{II}LSm^{III}(NO_3)_3]\cdot nCH_3COCH_3$ (4: n = 1; 4A: n = 0), $[Cu^{II}(H_2O)LLn^{III}(NO_3)_3]$ (5: Ln = Eu; 6: Ln = Gd), $[Cu^{II}LLn^{III}(NO_3)_3]$ (7−12: Ln = Tb−Yb), and $[Ni^{II}LLn^{III}(NO_3)_3]\cdot 0.5CH_3COCH_3$ (16−24: Ln = Sm−Yb). To a stirred suspension of $[Cu^{II}L\subset(H_2O)]$ or $[Ni^{II}L\subset(H_2O)]$ (0.122 g, 0.25 mmol) in acetone (15 mL) was added an acetone solution (5 mL) of 0.30 mmol of a hexahydrated or pentahydrated lanthanide(III) nitrate (lanthanide = Ce−Yb). The conversion of the suspension to a red colored solution takes place after addition of the lanthanide salt. After stirring for about 10 min, the solution was filtered to remove any suspended particles, and the red colored filtrate was kept at room temperature for slow evaporation. After time periods ranging between 24−48 h, for different compounds of the series, a red crystalline compound that deposited was collected by filtration and washed with cold acetone. Some of the crystalline compounds contained diffraction quality single crystals. The crystalline compound $[Cu^{II}LSm^{III}(NO_3)_3]\cdot CH_3COCH_3$ (**4**) loses solvated acetone quickly after its isolation and converts to $[Cu^{II}LSm^{III}(NO_3)_3]$ (**4A**). Yields: 80−90%. Observed/calculated elemental analyses and selected IR bands of **1**−**3**, **4A**, **5**, and **7**−**24** are listed in Supporting Information, Tables S1 and S2, respectively.

Crystal Structure Determination of Eight $Cu^{II}Ln^{III}$ Complexes (1−4: Ln = Ce−Sm; 7: Ln = Tb; 9: Ln = Ho; 10: Ln = Er; 12: Ln = Yb) and Three $Ni^{II}Ln^{III}$ Complexes (13: Ln = Ce; 16: Ln = Sm; 18: Ln = Gd). The crystallographic data of the eight $Cu^{II}Ln^{III}$ and three $Ni^{II}Ln^{III}$ complexes are summarized in Tables 1 and 2, respectively. Diffraction data of **9** and **13** were collected on a Bruker Nonius Kappa CCD diffractometer, while three different Bruker Apex-II Smart CCD diffractometers were used to collect data of other crystals. The data were collected at either of 100 K, 120 K, 193 K, and 296 K. The processed reflection data were corrected for Lorentz-polarization and background effects. Empirical absorption correction for **10** and **12** and multiscan absorption correction for the other structures have been applied. All six carbon atoms (C(10)−C(15)) of the cyclohexane moiety in **1**, **7**, **9**, and **13** were found as disordered over two sites with occupancies 0.49 and 0.51 for **1**, 0.77 and 0.23 for **7**, 0.68 and 0.32 for **9**, and 0.44 and 0.56 for **13**. In **2**, three carbon atoms (C(10), C(13), and C(15)) were found as disordered over two sites with occupancy values of either 0.50/0.50 or 0.58/0.42. Two nitrate oxygen atoms, O(51) and O(52), in **4** are also found as disordered over two sites with occupancy values of 0.65/0.35 and 0.50/0.50, respectively. It has not been possible to apply anisotropic refinement on C(10), C(13),

Table 2. Crystallographic Data for the Three $Ni^{II}Ln^{III}$ Complexes (**13**, **16**, and **18**)

	$Ni^{II}Ce^{III}$ (**13**)	$Ni^{II}Sm^{III}$ (**16**)	$Ni^{II}Gd^{III}$ (**18**)
empirical formula	$C_{24}H_{30}N_5O_{14}NiCe$	$C_{51}H_{62}N_{10}O_{27}Ni_2Sm_2$	$C_{51}H_{62}N_{10}O_{27}Ni_2Gd_2$
fw	811.36	1665.23	1679.03
crystal color	red	red	red
crystal system	monoclinic	monoclinic	monoclinic
space group	$P2_1/c$	$P2_1/c$	$P2_1/c$
a (Å)	14.406(2)	16.469(3)	16.458(4)
b (Å)	13.995(2)	24.389(4)	24.410(6)
c (Å)	15.826(2)	16.026(3)	15.984(4)
α (deg.)	90.00	90.00	90.00
β (deg.)	116.768(3)	108.909(5)	108.804(8)
γ (deg.)	90.00	90.00	90.00
V (Å^3)	2848.8(7)	6089.5(18)	6079(3)
Z	4	4	4
T, K	100(2)	296(2)	296(2)
2θ (deg.)	5.76−62.00	2.62−50.32	2.62−37.70
μ (mm^{-1})	2.319	2.604	2.858
ρ_{calcd} (g cm^{-3})	1.892	1.816	1.835
$F(000)$	1628	3336	3352
absorption correction	multi-scan	multi-scan	multi-scan
index ranges	$-20 \le h \le 20$	$-17 \le h \le 19$	$-14 \le h \le 14$
	$-19 \le k \le 20$	$-29 \le k \le 28$	$-21 \le k \le 22$
	$-22 \le l \le 22$	$-18 \le l \le 18$	$-14 \le l \le 14$
reflections collected	49238	69507	36658
independent reflections (R_{int})	9079(0.0641)	10768(0.1573)	4761(0.1601)
R_1[a]/ wR_2[b] ($I > 2\sigma(I)$)	0.0385/0.0816	0.0719/0.1669	0.0484/0.1201
R_1[a]/ wR_2[b] (for all data)	0.0590/0.0902	0.1410/0.2088	0.0876/0.1484

[a] $R_1 = [\sum||F_o| - |F_c||/\sum|F_o|]$. [b] $wR_2 = [\sum w(F_o^2 - F_c^2)^2/\sum wF_o^4]^{1/2}$.

and C(15) in **2** and **3** and on C(15), C(29), C(30), C(52), and C(56) in **18**, and therefore these carbon atoms were refined isotropically. All other nonhydrogen atoms in the eleven structures were refined anisotropically. Two water hydrogen atoms in each of **2** and **3** were not located, while those were located in **1** and **13**. It has not been possible to insert seven hydrogen atoms in **2** and two hydrogen atoms in **3**, of the cyclohexane moiety in both the cases. All other hydrogen atoms in the eleven structures were inserted at the geometrically calculated positions. As a better quality crystal of compound **18** was not obtained, the 2θ range (2.62−37.70°) of data collection is not sufficiently wide. All the crystal structures were determined by Direct methods, and subsequent Fourier and difference Fourier syntheses, followed by full-matrix least-squares refinements on F^2 using SHELXS-97 and SHELXL-97.[18] The final refinement converged at the R_1 ($I > 2\sigma(I)$) values of 0.0242, 0.0349, 0.0520, 0.0418, 0.0627, 0.0390, 0.0541, 0.0399, 0.0385, 0.0719, and 0.0484 for **1**, **2**, **3**, **4**, **7**, **9**, **10**, **12**, **13**, **16**, and **18**, respectively.

Results and Discussion

Description of the Structures of $[Cu^{II}LLn^{III}(NO_3)_3(H_2O)]$ (1−3: Ln = Ce−Nd), $[Ni^{II}LCe^{III}(NO_3)_3(H_2O)]$ (13), $[Cu^{II}LSm^{III}(NO_3)_3]\cdot CH_3COCH_3$ (4), $[Cu^{II}(H_2O)LGd^{III}(NO_3)_3]$ (6),[8a] $[Cu^{II}LLn^{III}(NO_3)_3]$ (7: Ln = Tb; 9: Ln = Ho; 10: Ln = Er; 12: Ln = Yb), and $[Ni^{II}LLn^{III}(NO_3)_3]\cdot 0.5CH_3COCH_3$ (16: Ln = Sm; 18: Ln = Gd). The structures of these twelve compounds reveal that all are diphenoxo-bridged $Cu^{II}Ln^{III}$ or $Ni^{II}Ln^{III}$ compounds. The inner salen-type N_2O_2 cavity is occupied by copper(II) or nickel(II), while lanthanide(III) is present in the open and larger O_4 compartment of the dinucleating compartmental ligand L^{2-}. The copper(II) center in the $Cu^{II}Gd^{III}$ (**6**) compound is pentacoordinated by the two imine nitrogen atoms, two bridging phenoxo oxygen atoms, and one water oxygen atom and thus adopts an approximate square pyramidal coordination environment; the water oxygen atom occupies the apical position.[8a] In contrast, in all the other eleven $M^{II}Ln^{III}$ structures, the copper(II) or nickel(II) center is tetracoordinated by the two imine nitrogen atoms and two bridging phenoxo oxygen atoms and thus adopts an approximate square planar coordination environment. In the eight structures involving heavier lanthanides starting from samarium(III), that is, in $Cu^{II}Sm^{III}$ (**4**), $Cu^{II}Gd^{III}$ (**6**), $Cu^{II}Tb^{III}$ (**7**), $Cu^{II}Ho^{III}$ (**9**), $Cu^{II}Er^{III}$ (**10**), $Cu^{II}Yb^{III}$ (**12**), $Ni^{II}Sm^{III}$ (**16**), and $Ni^{II}Gd^{III}$ (**18**), the lanthanide(III) center is ten-coordinated with two bridging phenoxo oxygen atoms, two ethoxy oxygen atoms, and two oxygen atoms of each of the three chelating nitrates. In contrast, the lanthanide(III) centers in the $Cu^{II}Ce^{III}$ (**1**), $Cu^{II}Pr^{III}$ (**2**), $Cu^{II}Nd^{III}$ (**3**), and $Ni^{II}Ce^{III}$ (**13**) complexes are eleven-coordinated because of the additional coordination by a water molecule. Again, the structures of the $Ni^{II}Sm^{III}$ (**16**) and $Ni^{II}Gd^{III}$ (**18**) compounds contain two independent units. The structures of the $Cu^{II}Ce^{III}$ (**1**), $Ni^{II}Ce^{III}$ (**13**), $Cu^{II}Sm^{III}$ (**4**), $Ni^{II}Sm^{III}$ (**16**, one unit), and $Cu^{II}Yb^{III}$ (**12**) complexes are shown in Figures 1−5, respectively, while those of the $Cu^{II}Pr^{III}$ (**2**), $Cu^{II}Nd^{III}$ (**3**), $Cu^{II}Tb^{III}$ (**7**), $Cu^{II}Ho^{III}$ (**9**), $Cu^{II}Er^{III}$ (**10**), $Ni^{II}Sm^{III}$ (**16**, two units), and $Ni^{II}Gd^{III}$ (**18**, two units) complexes are presented in Supporting Information, Figures S1−S7, respectively. Selected structural parameters of the eight $Cu^{II}Ln^{III}$ complexes and those of the previously published $Cu^{II}Gd^{III}$ (**6**)[8a] compound are summarized in Table 3, while the similar structural parameters of the $Ni^{II}Ce^{III}$ (**13**) complex, one unit of both the $Ni^{II}Sm^{III}$ (**16**) and the $Ni^{II}Gd^{III}$ (**18**) complexes are listed in Table 4. It may be noted that the $Cu^{II}Ce^{III}$ (**1**), $Cu^{II}Pr^{III}$ (**2**), $Cu^{II}Nd^{III}$ (**3**), and $Ni^{II}Ce^{III}$ (**13**) compounds belong to same space group $P2_1/c$ with similar values of the unit cell parameters, and therefore these four compounds are isomorphous. Similarly, the four compounds $Cu^{II}Tb^{III}$ (**7**),

(18) (a) Sheldrick, G. M. *SHELXS-97: A Program for Crystal Structure Solution*; University of Göttingen: Göttingen, Germany, 1997. (b) Sheldrick, G. M. *SHELXL-97: A Program for Crystal Structure Refinement*; University of Göttingen: Göttingen, Germany, 1993.

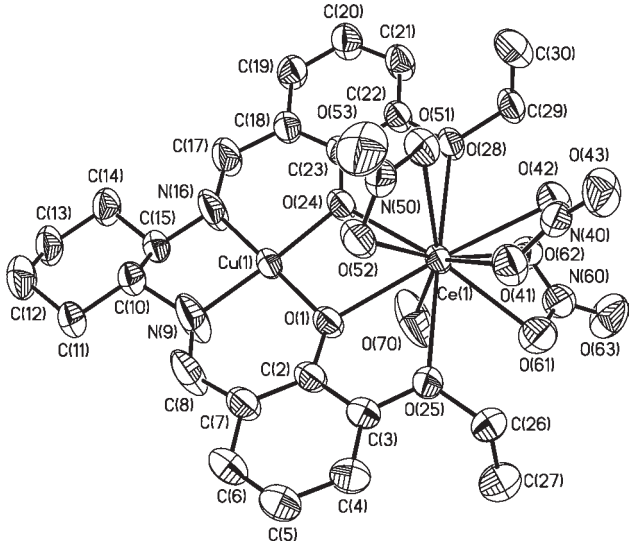

Figure 1. Crystal structure of $[Cu^{II}LCe^{III}(NO_3)_3(H_2O)]$ (**1**). Hydrogen atoms are omitted for clarity.

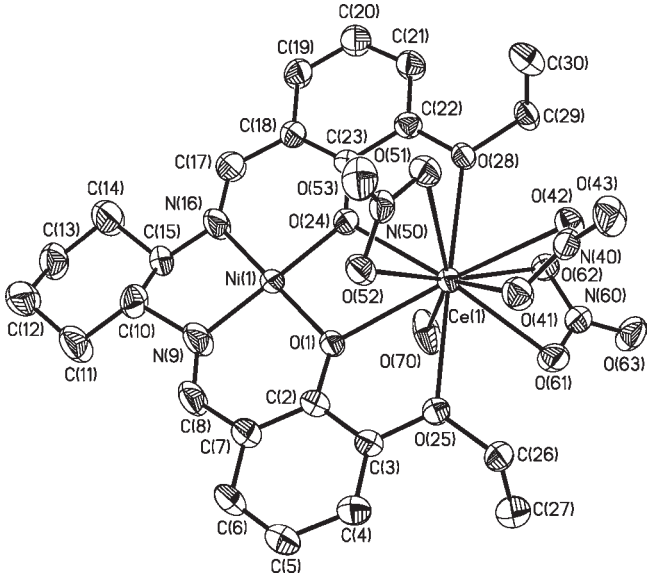

Figure 2. Crystal structure of $[Ni^{II}LCe^{III}(NO_3)_3(H_2O)]$ (**13**). Hydrogen atoms are omitted for clarity.

$Cu^{II}Ho^{III}$ (**9**), $Cu^{II}Er^{III}$ (**10**), and $Cu^{II}Yb^{III}$ (**12**) are isomorphous; the space group in this set is $P2_1/n$.

In the nine $Cu^{II}Ln^{III}$ structures, the Cu−N/O bond distances involving the N_2O_2 compartment lie in the range 1.881(4)−1.930(7) Å. In comparison, the Ni−N/O bond distances in the three $Ni^{II}Ln^{III}$ structures are slightly shorter and lie in the range 1.818(13)−1.872(2) Å. The *transoid* angles in the NiN_2O_2 environment of the $Ni^{II}Ln^{III}$ compounds are in between 176.1(4) and 177.66(14)°, while the range of the *transoid* angles in the CuN_2O_2 environment of the $Cu^{II}Ln^{III}$ structures are a little wider (168.44(12)−178.43(16)°). The *cisoid* angles in both the $Cu^{II}Ln^{III}$ and $Ni^{II}Ln^{III}$ compounds, however, vary in between about 82° and about 96°.

In the series from $Cu^{II}Ce^{III}$ to $Cu^{II}Yb^{III}$, both the Ln−O(phenoxo) bond distances, Ln−O(1) and Ln−O(24), decrease as the atomic number of the lanthanide increases; the Ce−O(phenoxo) distances are 2.5340(9)

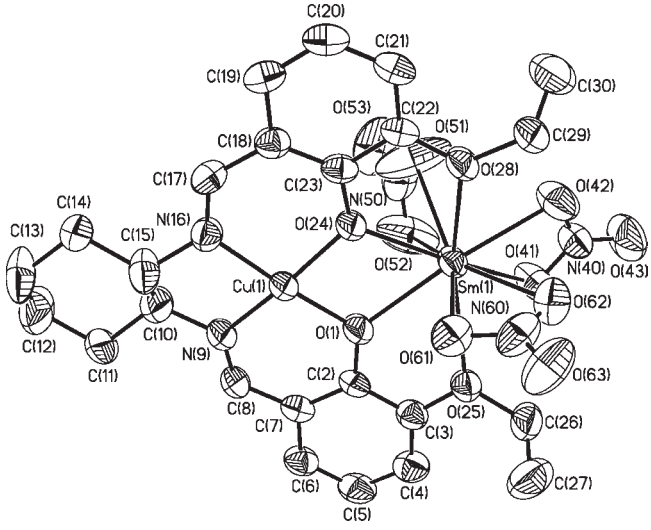

Figure 3. Crystal structure of $[Cu^{II}LSm^{III}(NO_3)_3]\cdot CH_3COCH_3$ (**4**). Acetone molecule and hydrogen atoms are omitted for clarity.

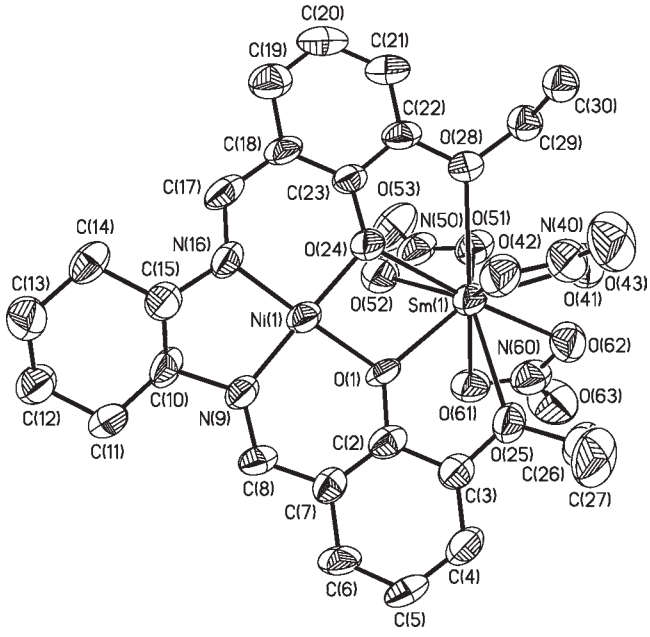

Figure 4. Crystal structure of one dinuclear unit (Unit 1) in $[Ni^{II}LSm^{III}(NO_3)_3]\cdot 0.5CH_3COCH_3$ (**16**). Acetone molecule and hydrogen atoms are omitted for clarity.

and 2.4763(10) Å, while the Yb−O(phenoxo) bond lengths are 2.259(3) and 2.253(3) Å. Similarly, a gradual decrease of one Ln−O(ethoxy) bond distance, which involves O(28), takes place from about 2.69 Å in $Cu^{II}Ce^{III}$/$Cu^{II}Pr^{III}$ to about 2.53 Å in $Cu^{II}Yb^{III}$. However, the change of the second Ln−O(ethoxy) bond length, which involves O(25), is not systematic in the series and varies in the range 2.641(2)−2.712(2) Å. A systematic variation is not also observed for the Ln−O(nitrate) bond distances in the $Cu^{II}Ln^{III}$ complexes. These bond distances lie in the range 2.355(4)−2.975(5) Å. In all these complexes, the Ln−O(phenoxo) bond distances are shorter than the bond lengths involving ethoxy and nitrate oxygen atoms. The Ln−O(water) bond lengths in the $Cu^{II}Ln^{III}$ (Ln = Ce, Pr, and Nd) complexes lie in the range of the Ln−O(phenoxo) distances.

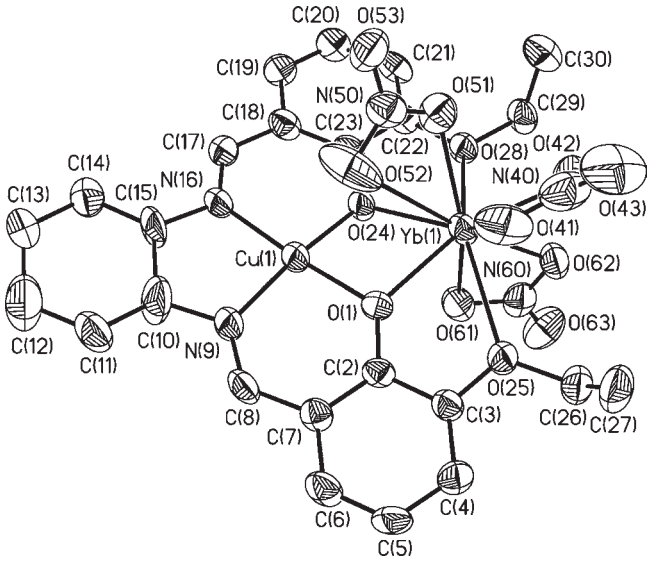

Figure 5. Crystal structure of $[Cu^{II}LYb^{III}(NO_3)_3]$ (**12**). Hydrogen atoms are omitted for clarity.

In the three $Ni^{II}Ln^{III}$ (Ln = Ce, Sm, and Gd) structures also, the Ln−O(phenoxo) bond lengths are shorter than the bond distances involving ethoxy and nitrate oxygen atoms. The Ce−O(water) bond length is close to Ce−O(phenoxo) bond distances as well. In contrast to that in the $Cu^{II}Ln^{III}$ complexes, all the corresponding Ln−O bond distances in the three $Ni^{II}Ln^{III}$ structures decrease systematically with the increase of the atomic number of lanthanides. The ranges of the Ln−O(phenoxo), Ln−O(ethoxy), and Ln−O(nitrate) bond distances in the $Ni^{II}Ce^{III}$ complex are 2.5055(19)−2.5556(19) Å, 2.6550(19)−2.657(2) Å, and 2.573(2)−2.681(2) Å, while those in the $Ni^{II}Gd^{III}$ complex are 2.334(10)−2.440(11) Å, 2.554(11)−2.636(10) Å, and 2.465(11)−2.510(11) Å.

The copper(II)···lanthanide(III) separation in the $Cu^{II}Ln^{III}$ complexes decreases systematically from 3.54 Å in the Ce^{III} system to 3.26 Å in the Yb^{III} system. A similar trend is also observed for the nickel(II)···lanthanide(III) separation in the three $Ni^{II}Ln^{III}$ complexes (Ni···Ce = 3.57 Å and Ni···Gd = 3.42 Å). Although the Cu−phenoxo−Ln bridge angles in the $Cu^{II}Ln^{III}$ series are not varied systematically, an overall decrease of both the bridge angles from the Ce^{III} system (105.19(4) and 106.67(4)°) to the Yb^{III} system (102.48(14) and 103.28(15)°) takes place. With the increase of the atomic number of the lanthanides in the three $Ni^{II}Ln^{III}$ complexes, while one bridge angle decreases systematically (108.44(9) and 104.8(5)° in the Ce^{III} and Gd^{III} complexes, respectively), the second angle increases gradually from 106.86(8)° in the Ce^{III} complex to 108.7(5)° in the Gd^{III} complex.

The extent of planarity of the $MO(phenoxo)_2Ln$ bridging cores can be understood from the dihedral angle (δ) between the $MO(phenoxo)_2$ and $LnO(phenoxo)_2$ planes. As already discussed, the $CuO(phenoxo)_2Gd$ bridging core in the $Cu^{II}Gd^{III}$ complex is almost planar ($\delta = 2.1°$). The bridging cores are more planar in the $Cu^{II}Ce^{III}$, $Cu^{II}Pr^{III}$, $Cu^{II}Nd^{III}$, and $Ni^{II}Ce^{III}$ complexes as evidenced by the δ values of 0.8, 1.0, 1.5, and 1.3°, respectively. In the $Cu^{II}Sm^{III}$ complex (**4**, $\delta = 6.2°$), the bridging moiety is slightly twisted. In comparison, the bridging core is more twisted in the $Ni^{II}Sm^{III}$ ($\delta = 13.8$ and 15.5° for the two units), $Ni^{II}Gd^{III}$ ($\delta = 13.7$ and 15.0° for the two units), $Cu^{II}Tb^{III}$ ($\delta = 18.4°$), $Cu^{II}Ho^{III}$ ($\delta = 17.6°$), $Cu^{II}Er^{III}$ ($\delta = 19.1°$), and $Cu^{II}Yb^{III}$ ($\delta = 19.1°$) complexes. Clearly, while the bridging moieties in the $Cu^{II}Ln^{III}$ complexes involving lower lanthanides are either almost planar (Ce, Pr, Nd, and Gd; $\delta = 0.8-2.1°$) or slightly twisted (for Sm; $\delta = 6.2°$), those in the higher analogues are significantly twisted (for Tb, Ho, Er, and Yb; $\delta = 17.6-19.1°$).

Intermolecular copper···lanthanide, copper···copper, and lanthanide···lanthanide separations in the nine $Cu^{II}Ln^{III}$ structures lie in the ranges 7.17−8.36 Å, 6.32−7.42 Å, and 7.83−8.97 Å, respectively, indicating that the dinuclear 3d−4f cores are well separated. As the intermolecular metal···metal distances in the $Ni^{II}Ce^{III}$ complex are greater than 7 Å, this system is also discrete dinuclear. In the cases of the $Ni^{II}Sm^{III}$ and $Ni^{II}Gd^{III}$ complexes, although Ni···Ln and Ln···Ln separations vary between 7.19 and 8.36 Å, the distances between the nickel(II) centers of the two independent units are relatively smaller, about 4.71 Å. However, as this distance is greater than 3.5 Å, supramolecular nickel(II)···nickel(II) interaction in these cases is not possible.[19] The possibility of very weak magnetic interaction between the dinuclear cores in these two complexes, $Ni^{II}Sm^{III}$ and $Ni^{II}Gd^{III}$, can also be discarded because of the diamagnetic nature of the nickel(II) centers (vide infra).

The structures of three pairs of $Cu^{II}Ln^{III}$ and $Ni^{II}Ln^{III}$ complexes, involving the same lanthanides (Ce, Sm, and Gd), have been determined. The $Cu^{II}Ce^{III}$ and the $Ni^{II}Ce^{III}$ complexes have same $P2_1/c$ space group with almost identical unit cell parameters, and therefore this pair is isomorphous. Comparison of bond lengths involving the lanthanide(III) center in the $Ni^{II}Ce^{III}$ and $Cu^{II}Ce^{III}$ compounds reveal that the corresponding bond lengths differ by a maximum of 0.04 Å (Supporting Information, Table S3). Although the space group of the $Cu^{II}Sm^{III}$ and the $Ni^{II}Sm^{III}$ complexes are same, $P2_1/c$, the unit cell parameters of the two complexes are significantly different, indicating that this pair is not isomorphous. The $Cu^{II}Gd^{III}$ and $Ni^{II}Gd^{III}$ pair is also not isomorphous because of different space groups, triclinic $P\bar{1}$ and monoclinic $P2_1/c$, respectively. Comparison of the bond lengths involving the lanthanide(III) centers in the $Cu^{II}Sm^{III}$ and two units of $Ni^{II}Sm^{III}$ (Supporting Information, Table S4) as well as in the $Cu^{II}Gd^{III}$ and two units of $Ni^{II}Gd^{III}$ (Supporting Information, Table S5) complexes reveal that difference for most of the corresponding bond lengths is less than 0.05 Å; the difference in only one bond distance involving one phenoxo oxygen in both cases is only slightly greater, 0.07 Å for Sm^{III} and 0.1 Å for Gd^{III}.

Syntheses, Characterization, and Composition. The mononuclear compounds, $[Cu^{II}L\subset(H_2O)]$[8a] and $[Ni^{II}L\subset(H_2O)]$, are readily prepared by reacting H_2L with metal acetates in MeOH-water followed by recrystallization from *N*,*N*′-dimethylformamide. The heterodinuclear $M^{II}Ln^{III}$ complexes (**1**−**12**: M = Cu, Ln = Ce−Yb; **13**−**24**: M = Ni, Ln = Ce−Yb) are smoothly produced in high yield on treatment of the mononuclear compounds, $[Cu^{II}L\subset(H_2O)]$

(19) (a) Nayak, M.; Jana, A.; Fleck, M.; Hazra, S.; Mohanta, S. *CrystEngComm.* **2010**, *5*, 1416–1421. (b) Siegler, M. A.; Lutz, M. *Cryst. Growth Des.* **2009**, *9*, 1194–1200. (c) Thomas, W.; Underhill, A. E. *Chem. Soc. Rev.* **1972**, *1*, 99–120.

Table 3. Selected Structural Parameters[a] of the Nine $Cu^{II}Ln^{III}$ Complexes (**1**−**4**, **6**, **7**, **9**, **10**, and **12**)

	$Cu^{II}Ce^{III}$ (**1**)	$Cu^{II}Pr^{III}$ (**2**)	$Cu^{II}Nd^{III}$ (**3**)	$Cu^{II}Sm^{III}$ (**4**)	$Cu^{II}Gd^{III}$ (**6**)	$Cu^{II}Tb^{III}$ (**7**)	$Cu^{II}Ho^{III}$ (**9**)	$Cu^{II}Er^{III}$ (**10**)	$Cu^{II}Yb^{III}$ (**12**)
Ln(1)−O(1)	2.5340(9)	2.529(2)	2.524(5)	2.383(4)	2.380(2)	2.329(4)	2.294(2)	2.290(4)	2.259(3)
Ln(1)−O(24)	2.4763(10)	2.471(2)	2.465(5)	2.393(3)	2.343(2)	2.312(4)	2.292(2)	2.290(4)	2.253(3)
Ln(1)−O(25)	2.6915(10)	2.693(2)	2.690(5)	2.691(4)	2.712(2)	2.670(4)	2.641(2)	2.661(4)	2.661(3)
Ln(1)−O(28)	2.6925(10)	2.694(2)	2.688(5)	2.626(4)	2.568(2)	2.588(4)	2.559(2)	2.558(4)	2.535(3)
Ln(1)−O(70)	2.5045(12)	2.509(3)	2.486(6)						
Ln(1)−O(nitrate)	2.5677(11)−2.7242(12)	2.564(3)−2.760(3)	2.545(5)−2.706(6)	2.460(19)−2.541(5)	2.450(3)−2.554(3)	2.434(4)−2.641(5)	2.387(3)−2.642(3)	2.381(5)−2.847(6)	2.355(4)−2.975(5)
Cu(1)−O(1)	1.8991(10)	1.898(2)	1.896(5)	1.910(4)	1.915(2)	1.899(4)	1.897(2)	1.907(4)	1.913(3)
Cu(1)−O(24)	1.9206(10)	1.923(2)	1.922(5)	1.907(3)	1.909(2)	1.895(4)	1.883(2)	1.881(4)	1.895(3)
Cu(1)−N(9)	1.9187(13)	1.925(3)	1.930(7)	1.915(5)	1.918(3)	1.909(5)	1.901(3)	1.899(6)	1.907(4)
Cu(1)−N(16)	1.9035(15)	1.912(3)	1.897(7)	1.916(4)	1.922(3)	1.898(5)	1.904(3)	1.915(6)	1.910(4)
Cu(1)−O(water)					2.535(3)				
O(1)−Cu(1)−N(16)	177.57(8)	178.43(16)	177.1(3)	174.60(18)	178.41(11)	171.9(2)	172.55(14)	173.5(2)	173.27(18)
O(24)−Cu(1)−N(9)	174.47(7)	174.59(15)	174.1(3)	169.02(19)	168.44(12)	172.9(2)	172.92(14)	172.1(2)	170.67(18)
O(1)−Cu(1)−N(9)	95.02(5)	95.05(12)	95.1(3)	94.55(18)	94.47(10)	94.95(19)	94.94(12)	94.7(2)	95.23(17)
O(1)−Cu(1)−O(24)	85.69(4)	85.45(10)	85.4(2)	83.32(15)	84.23(9)	83.07(17)	83.23(10)	83.40(19)	82.55(14)
O(24)−Cu(1)−N(16)	94.95(5)	95.16(12)	95.1(3)	95.24(17)	94.59(10)	95.8(2)	94.93(12)	95.6(2)	96.35(17)
N(9)−Cu(1)−N(16)	84.57(6)	84.49(14)	84.6(3)	85.87(19)	86.47(11)	87.1(2)	87.74(13)	87.1(3)	86.90(18)
Cu(1)−O(1)−Ln(1)	105.19(4)	105.35(9)	105.3(2)	106.19(16)	104.18(9)	103.35(17)	103.20(10)	102.47(18)	102.48(14)
Cu(1)−O(24)−Ln(1)	106.67(4)	106.75(9)	106.7(2)	105.88(14)	105.77(9)	104.10(17)	103.73(10)	103.32(19)	103.28(15)
δ^b	0.8	1.0	1.5	6.2	2.1	18.4	17.6	19.1	19.1
Cu···Ln[c]	3.5426(4)	3.5408(5)	3.534	3.4442(7)	3.401	3.3276(8)	3.2936(5)	3.281	3.260
Cu···Cu[d]	7.149	7.253	7.164	7.418	6.469	6.323	6.316	6.346	6.390
Ln···Ln[d]	7.833	7.896	7.838	8.967	8.607	8.533	8.525	8.564	8.588
Cu···Ln[d]	7.174	7.237	7.191	8.362	7.657	7.329	7.304	7.306	7.310

[a] Distances in Å and angles in deg. [b] Dihedral angle between $CuO(phenoxo)_2$ and $LnO(phenoxo)_2$ planes. [c] Intramolecular. [d] Intermolecular.

Table 4. Selected Structural Parameters[a] of the Three $Ni^{II}Ln^{III}$ Complexes (**13**, **16**, and **18**)

	$Ni^{II}Ce^{III}$ (**13**)	$Ni^{II}Sm^{III}$ (**16**), Unit I	$Ni^{II}Gd^{III}$ (**18**),Unit I
Ln(1)−O(1)	2.5556(19)	2.358(7)	2.334(10)
Ln(1)−O(24)	2.5055(19)	2.462(7)	2.440(11)
Ln(1)−O(25)	2.657(2)	2.656(8)	2.636(10)
Ln(1)−O(28)	2.6550(19)	2.585(7)	2.554(11)
Ln(1)−O(70)	2.501(2)		
Ln(1)−O(nitrate)	2.573(2)−2.681(2)	2.469(9)−2.523(8)	2.465(11)−2.510(11)
Ni(1)−O(1)	1.8605(19)	1.868(7)	1.860(10)
Ni(1)−O(24)	1.872(2)	1.840(7)	1.850(11)
Ni(1)−N(9)	1.851(3)	1.840(9)	1.848(13)
Ni(1)−N(16)	1.833(3)	1.830(8)	1.818(13)
O(1)−Ni(1)−N(16)	177.66(14)	177.4(4)	177.5(5)
O(24)−Ni(1)−N(9)	177.55(12)	176.1(4)	176.5(5)
O(1)−Ni(1)−N(9)	94.82(10)	95.0(3)	95.8(6)
O(1)−Ni(1)−O(24)	84.95(8)	82.7(3)	82.3(5)
O(24)−Ni(1)−N(16)	95.05(10)	95.4(4)	96.1(6)
N(9)−Ni(1)−N(16)	85.28(12)	86.9(4)	85.8(7)
Ni(1)−O(1)−Ln(1)	106.86(8)	108.3(3)	108.7(5)
Ni(1)−O(24)−Ln(1)	108.44(9)	105.1(3)	104.8(5)
δ^b	1.3	15.5	15.0
Ni···Ln[c]	3.5707(6)	3.4361(17)	3.419
Ni···Ni[d]	7.070	4.709	4.718
Ln···Ln[d]	7.915	8.358	8.348
Ni···Ln[d]	7.374	7.199	7.186

[a] Distances in Å and angles in deg. [b] Dihedral angle between $NiO(phenoxo)_2$ and $LnO(phenoxo)_2$ planes. [c] Intramolecular. [d] Intermolecular.

or $[Ni^{II}L\subset(H_2O)]$, with hydrated lanthanide(III) nitrates in acetone.

The characteristic C═N stretching of $[Cu^{II}L\subset(H_2O)]$ and $[Ni^{II}L\subset(H_2O)]$ appears as a strong band at 1623 and 1618 cm^{-1}, respectively, while this vibration in the twenty four $M^{II}Ln^{III}$ complexes is observed, also as a strong signal, in the range 1620−1639 cm^{-1}. The presence of nitrates in the $M^{II}Ln^{III}$ complexes is evidenced by a strong signal at about 1384 cm^{-1}. Two medium intensity bands at 3541 and 3501 cm^{-1} for $[Cu^{II}L\subset(H_2O)]$[8a] and 3577 and 3527 cm^{-1} for $[Ni^{II}L\subset(H_2O)]$ are indicative that the water molecules in these molecules are encapsulated in the O_4 compartment of the ligand to form the inclusion products.[20] While syntheses and characterization of $[Cu^{II}L\subset(H_2O)]$[8a] has been reported previously, $[Ni^{II}L\subset(H_2O)]$ is a new compound which has been characterized by elemental analyses, FT-IR, and single crystal X-ray structure determination (see Supporting Information). Each of the $M^{II}Ln^{III}$ (**1**−**3**: M = Cu, Ln = Ce−Nd; **13**−**15**: M = Ni, Ln = Ce−Nd) complexes exhibit one medium intensity band in the range 3370−3465 cm^{-1}, indicating the presence of a water molecule. The presence of a water molecule, coordinated to the lanthanide(III) center, in the structures of **1**−**3** and **13** has been already discussed. The elemental analyses of the six compounds **1**−**3** and **13**−**15** are also well matched with the formula containing one water molecule. Combining all these, it can be concluded that the composition of these six compounds is $[M^{II}LLn^{III}(NO_3)_3(H_2O)]$ (M = Cu or Ni, Ln = Ce−Nd).

The $Ni^{II}Ln^{III}$ compounds (**16**−**24**: Ln = Sm−Yb) exhibit one weak intensity band at about 1720 cm^{-1}. As already discussed, the structures of the $Ni^{II}Sm^{III}$ and $Ni^{II}Gd^{III}$ compounds contain half of an acetone molecule per $[Ni^{II}LLn^{III}(NO_3)_3]$ dinuclear moiety. Elemental analyses of the $Ni^{II}Sm^{III}$ and $Ni^{II}Gd^{III}$ as well as other $Ni^{II}Ln^{III}$ (Ln = Eu, Tb−Yb) compounds are well matched with the composition $[Ni^{II}LLn^{III}(NO_3)_3]\cdot 0.5CH_3COCH_3$. Clearly, the composition of these $Ni^{II}Ln^{III}$ complexes can be logically formulated as $[Ni^{II}LLn^{III}(NO_3)_3]\cdot 0.5CH_3COCH_3$, and the weak intensity band at about 1720 cm^{-1} can be assigned to the carbonyl stretching of the solvated acetone molecule.

Among six $Cu^{II}Ln^{III}$ complexes involving $4f^{8-13}$ lanthanides, the compositions of the structures of the four (Tb, Ho, Er, and Yb analogues) are $[Cu^{II}LLn^{III}(NO_3)_3]$. The elemental analyses of these four as well as those of the remaining two, $Cu^{II}Dy^{III}$ and $Cu^{II}Tm^{III}$, complexes are matched with the similar compositions and therefore these six compounds can be formulated as $[Cu^{II}LLn^{III}(NO_3)_3]$.

The composition of the structure of the $Cu^{II}Sm^{III}$ (**4**) compound is $[Cu^{II}LSm^{III}(NO_3)_3]\cdot CH_3COCH_3$. However, no peak due to carbonyl stretching is observed in its IR spectrum. Moreover, its elemental analyses are well matched with the composition $[Cu^{II}LSm^{III}(NO_3)_3]$. Clearly, $[Cu^{II}LSm^{III}(NO_3)_3]\cdot CH_3COCH_3$ (**4**) crystal loses the solvent molecule to form $[Cu^{II}LSm^{III}(NO_3)_3]$ (**4A**). Obviously, elemental analyses and IR spectroscopic and magnetic studies of **4A**, not of **4**, have been performed. However, the metrical parameters of the bridging core of **4A** can be logically approximated as those of **4**.

The $Cu^{II}Eu^{III}$ compound exhibits one band of medium intensity at 3350 cm^{-1}, which can be assigned to water stretchings. The elemental analyses of this compound are also matched with a composition containing one Cu^{II}, one Eu^{III}, three NO_3^-, and one H_2O molecule. The water may be coordinated to copper(II) or europium(III), or it may exist as solvent of crystallization. As discussed, the $Cu^{II}Ln^{III}$ complexes of Ce, Pr, and Nd contain a water molecule coordinated to the lanthanide, whereas the $Cu^{II}Sm^{III}$ structure contains no water molecule. On the other hand, the composition of the previously reported $Cu^{II}Gd^{III}$ compound is $[Cu^{II}(H_2O)LGd^{III}(NO_3)_3]$.[8a]

(20) (a) Nayak, M.; Koner, R.; Lin, H.-H.; Flörke, U.; Wei, H.-H.; Mohanta, S. *Inorg. Chem.* **2006**, *45*, 10764–10773. (b) Nayak, M.; Hazra, S.; Lemoine, P.; Koner, R.; Lucas, C. R.; Mohanta, S. *Polyhedron* **2008**, *27*, 1201–1213.

Therefore, it is more logical to formulate the $Cu^{II}Eu^{III}$ compound as $[Cu^{II}(H_2O)LEu^{III}(NO_3)_3]$.

Evidently, the variation in composition takes place for the 3d−4f compounds in the present investigation. Four types of composition are observed in the $Cu^{II}Ln^{III}$ complexes: $[Cu^{II}LLn^{III}(NO_3)_3(H_2O)]$ (**1**−**3**: Ln = Ce−Nd), $[Cu^{II}LSm^{III}(NO_3)_3]\cdot CH_3COCH_3$ (**4**), $[Cu^{II}(H_2O)LLn^{III}(NO_3)_3]$ (**5**: Ln = Eu; **6**: Ln = Gd), and $[Cu^{II}LLn^{III}(NO_3)_3]$ (**4A**: Ln = Sm; **7**−**12**: Ln = Tb−Yb). The $Ni^{II}Ln^{III}$ complexes are characterized to have two types of composition: $[Ni^{II}LLn^{III}(H_2O)(NO_3)_3]$ (**13**−**15**: Ln = Ce−Nd) and $[Ni^{II}LLn^{III}(NO_3)_3]\cdot 0.5CH_3COCH_3$ (**16**−**24**: Ln = Sm−Yb).

We would like to mention also that although both the $Cu^{II}Ln^{III}$ and the $Ni^{II}Ln^{III}$ complexes are produced in crystalline form, the diffraction quality single crystalline nature of the nickel(II) analogues is poor in most cases, except those with the lower three members (Ce, Pr, and Nd). Regarding the $Ni^{II}Ln^{III}$ compounds having $4f^{4-13}$ lanthanides, it has only been possible to isolate the single crystals of the samarium(III) and gadolinium(III) analogues, the later of which did not diffract well. However, as discussed above, the compositions of all the complexes can be reasonably formulated from the results of elemental analyses, IR spectra, and X-ray structures of some systems.

Magnetic Properties. Variable-temperature magnetic susceptibility of all twenty four unblocked samples were measured. Where necessary, samples were additionally measured on blocking with grease (blocked samples). The nature of magnetic exchange interaction has been understood utilizing the empirical approach. It may be mentioned that the empirical approach can be applied well for the title compounds to understand the nature of exchange interaction (for discussion in detail, see the Supporting Information).[11−15]

We guessed the powder reorientations in some samples on observing either of the followings in the unblocked data: (1) in comparison to the theoretical value of the noncorrelated spin combination, unusually higher $\chi_M T$ or $\Delta\chi_M T$ value at 300 K; (2) greater $\chi_M T$ values of a $Ni^{II}Ln^{III}$ complex than in the corresponding $Cu^{II}Ln^{III}$ complex; (3) unstraightforward or unusual $\Delta\chi_M T$ versus T profile resulting in either no conclusion or an unusual nature of interaction. Both the unblocked and the blocked data for the Ce^{III} and Tb^{III} complexes, as representative examples, are described below to demonstrate the effect of powder reorientations. For other cases, we report the blocked data only where orientation effects may influence the magnetic data. Where no significant differences are expected or observed, we report the unblocked data to avoid possible errors that may arise from the diamagnetic contributions because of the use of the grease. We thus simply avoid possible mistakes in the diamagnetic corrections.

The $\chi_M T/\Delta\chi_M T$ versus T profiles of the twenty four complexes are shown in Figures 6−14 and Supporting Information, Figures S9−S13, while the $\chi_M T/\Delta\chi_M T$ values at 300 K along with the theoretical $\chi_M T$ values for the noncorrelated spin combinations are listed in Table 5. The unit of $\chi_M T$ and $\Delta\chi_M T$ in the discussion below is $cm^3\ mol^{-1}$ K.

$\chi_M T/\Delta\chi_M T$ versus T Profiles of the $Cu^{II}Ce^{III}$ (1) and $Ni^{II}Ce^{III}$ (13) Complexes. $\chi_M T$ and $\Delta\chi_M T$ versus T plots, both blocked and unblocked, of the Ce^{III} complexes are shown in Figures 6 and 7, respectively. In the case of $Cu^{II}Ce^{III}$ (**1**), unblocked $\chi_M T$ increases slightly in the temperature range 300−75 K and decreases gradually in the temperature range 75−2 K. On the other hand, unblocked $Ni^{II}Ce^{III}$ (**13**) complex exhibits steady decrease of $\chi_M T$ on lowering of temperature. As shown in Figure 7, unblocked $\Delta\chi_M T$ of Ce^{III} gradually increases from 0.56 at 300 K to reach a saturation value of 0.75 in the temperature range 20−6 K. On further cooling, $\Delta\chi_M T$ only slightly decreases to 0.66 at 2 K. Therefore it seems from the unblocked data that the interaction between Cu^{II} and Ce^{III} is ferromagnetic, which is unusual because ferromagnetic interaction in a $4f^{1-6}$ lanthanide containing complex is not known. To check whether this anomaly is the inherent nature of the material or arises because of powder reorientation, we collected data of both the $Cu^{II}Ce^{III}$ and the $Ni^{II}Ce^{III}$ complexes on blocking the samples with grease. As shown in Figure 6, the $\chi_M T$ values

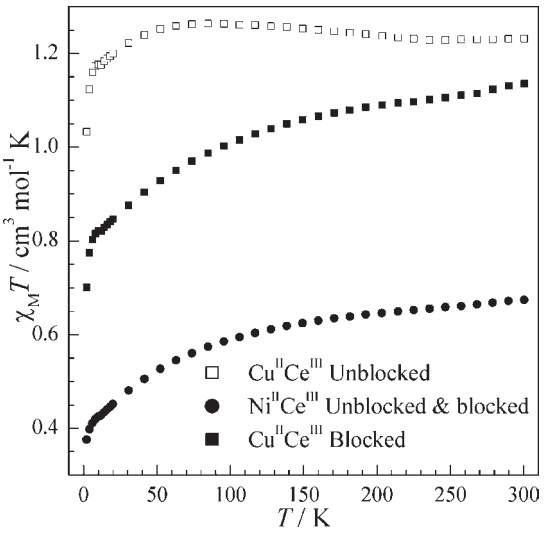

Figure 6. Temperature dependence of blocked and unblocked $\chi_M T$ for **1** ($Cu^{II}Ce^{III}$) and **13** ($Ni^{II}Ce^{III}$).

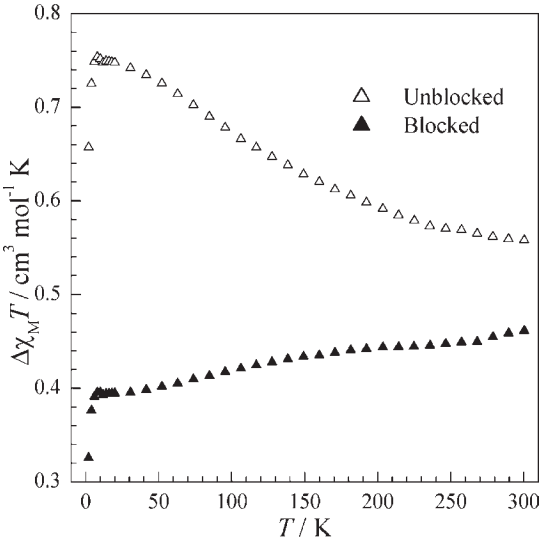

Figure 7. Temperature dependence of blocked and unblocked $\Delta\chi_M T$ between the susceptibilities of **1** ($Cu^{II}Ce^{III}$) and **13** ($Ni^{II}Ce^{III}$).

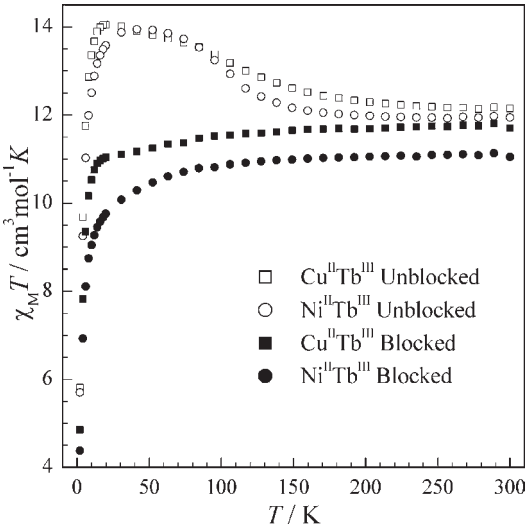

Figure 8. Temperature dependence of blocked and unblocked $\chi_M T$ for **7** ($Cu^{II}Tb^{III}$) and **19** ($Ni^{II}Tb^{III}$).

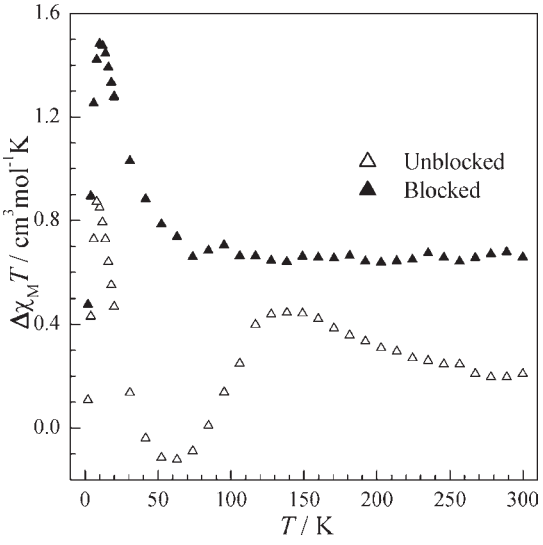

Figure 9. Temperature dependence of blocked and unblocked $\Delta\chi_M T$ between the susceptibilities of **7** ($Cu^{II}Tb^{III}$) and **19** ($Ni^{II}Tb^{III}$).

of the blocked $Cu^{II}Ce^{III}$ sample are smaller than those of the unblocked sample throughout the temperature range, and the blocked data decreases gradually from 300 to 2 K, indicating significant powder reorientation effect of this complex. On the other hand, the blocked and unblocked data of the $Ni^{II}Ce^{III}$ complex are practically superimposible (one set is shown in Figure 6), indicating that no reorientation takes place in this sample. $\Delta\chi_M T$ versus T profile, Figure 7, decreases slowly from 0.46 to 0.39 in the temperature range 300−10 K and then sharply decreases to 0.32 at 2 K, indicating antiferromagnetic interaction between copper(II) and cerium(III). Clearly, sharp increase of $\Delta\chi_M T$ of the unblocked data (Figure 7) arises because of powder reorientation of the unblocked Cu^{II}-Ce^{III} complex; while the interaction seems to be ferromagnetic on the basis of unblocked data, the metal centers are actually coupled by weak antiferromagnetic interaction.

$\chi_M T/\Delta\chi_M T$ versus T Profiles of the $Cu^{II}Tb^{III}$ (7) and $Ni^{II}Tb^{III}$ (19) Complexes. As shown in Figure 8, the

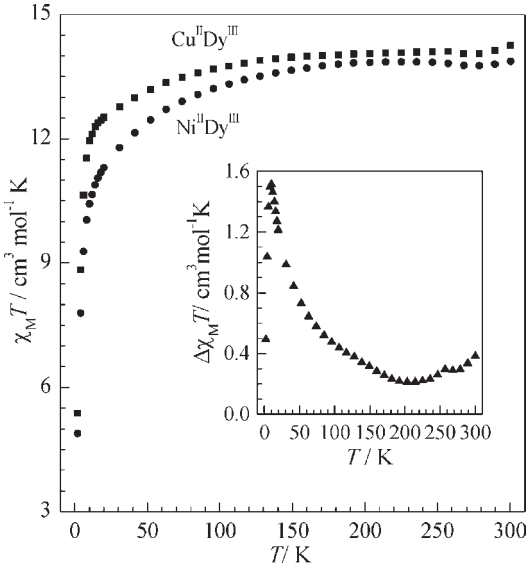

Figure 10. Temperature dependence of blocked $\chi_M T$ for **8** ($Cu^{II}Dy^{III}$) and **20** ($Ni^{II}Dy^{III}$). $\Delta\chi_M T$ versus T profile is shown in the inset.

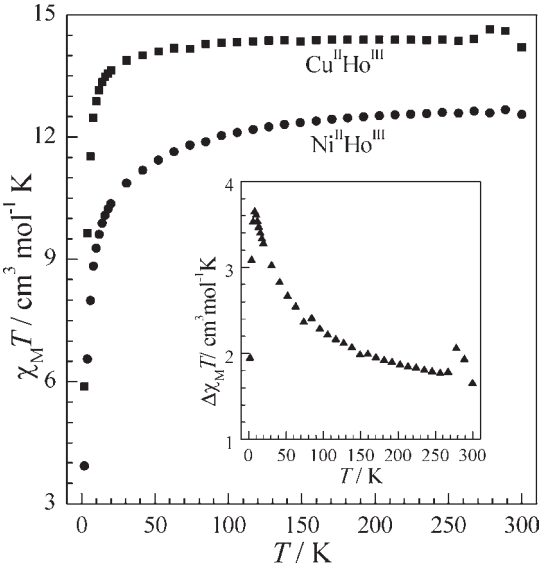

Figure 11. Temperature dependence of blocked $\chi_M T$ for **9** ($Cu^{II}Ho^{III}$) and **21** ($Ni^{II}Ho^{III}$). $\Delta\chi_M T$ versus T profile is shown in the inset.

unblocked $\chi_M T$ versus T profiles of the $Cu^{II}Tb^{III}$ and $Ni^{II}Tb^{III}$ complexes are very much similar except for slight change of the values. Moreover, the unblocked $\Delta\chi_M T$ versus T profile is too zigzag to make any conclusion (Figure 9). Therefore, powder reorientation was guessed, and the data of both the complexes were collected on blocking with grease. Significant change of magnetic data of the Tb^{III} complexes takes place on blocking. The $\chi_M T$ of both the blocked samples decreases throughout the temperature range, Figure 8; slow decrease from 300 K to a particular lower temperature (18 K for **7**, 42 K for **19**) followed by rapid decrease. As compared in Figure 8, the anomalies in the $\chi_M T$ of the unblocked samples are removed in the $\chi_M T$ of the blocked samples. Moreover, the $\Delta\chi_M T$ versus T profile becomes straightforward on blocking (Figure 9). While the $\Delta\chi_M T$ versus T profile of the unblocked sample is very much zigzag, $\Delta\chi_M T$ of blocked sample remains constant in the

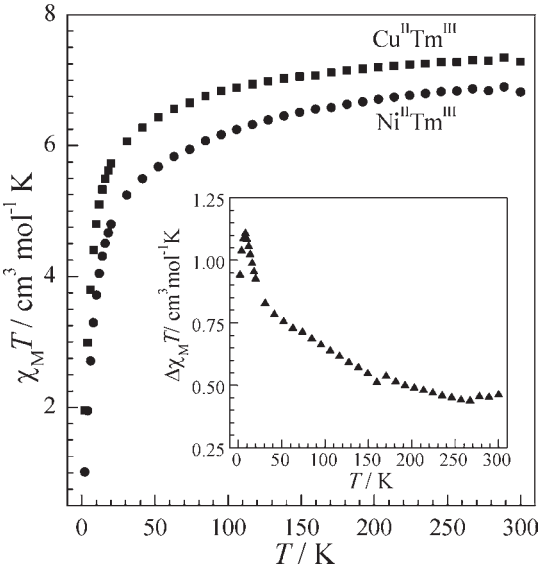

Figure 12. Temperature dependence of blocked $\chi_M T$ for **11** ($Cu^{II}Tm^{III}$) and **23** ($Ni^{II}Tm^{III}$). $\Delta\chi_M T$ versus T profile is shown in the inset.

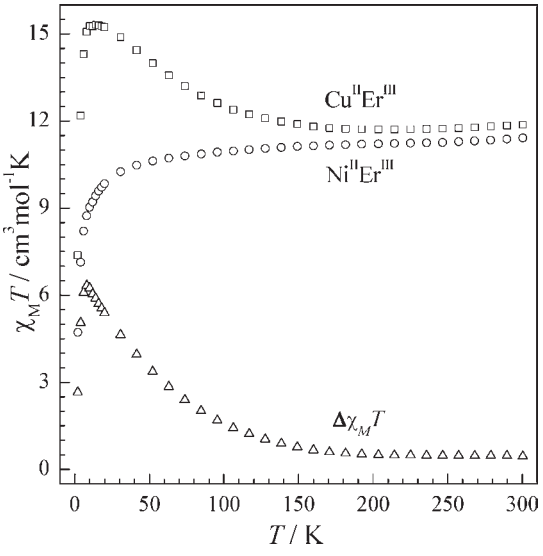

Figure 13. Temperature dependence of unblocked $\chi_M T$ for **10** ($Cu^{II}Er^{III}$) and **22** ($Ni^{II}Er^{III}$) and $\Delta\chi_M T$ between the susceptibilities of these two compounds.

temperature range 300−75 K, increases rapidly in the temperature range 75−10 K, and then decreases rapidly up to 2 K. The profile clearly indicates ferromagnetic interaction in the $Cu^{II}Tb^{III}$ complex.

$\chi_M T/\Delta\chi_M T$ versus T Profiles of the $Cu^{II}Ln^{III}$ and $Ni^{II}Ln^{III}$ Complexes (Ln = Pr−Eu; 2, 3, 4A, 5, and 14−17). $\chi_M T$ and $\Delta\chi_M T$ versus T plots of the Pr^{III} (blocked), Nd^{III} (blocked), Sm^{III} (unblocked), and Eu^{III} (unblocked) complexes are shown in Supporting Information, Figures S9−S12. All eight compounds exhibit decrease of $\chi_M T$ on lowering of temperature from 300 to 2 K. However, the decreasing patterns are of different types. $\chi_M T$ diminishes equally steadily throughout the temperature range for $Ni^{II}Eu^{III}$ (**17**) and $Cu^{II}Eu^{III}$ (**5**), while the $\chi_M T$ versus T profile is linear for $Ni^{II}Sm^{III}$ (**16**). On the other hand, slow decrease up to a particular temperature (T_X) followed by rapid decrease up to 2 K is observed for $Cu^{II}Pr^{III}$ (**2**; T_X = 75 K), $Ni^{II}Pr^{III}$ (**14**; T_X = 55 K), $Cu^{II}Nd^{III}$ (**3**; T_X = 50 K), $Ni^{II}Nd^{III}$ (**15**; T_X = 40 K), and $Cu^{II}Sm^{III}$ (**4A**; T_X = 20 K).

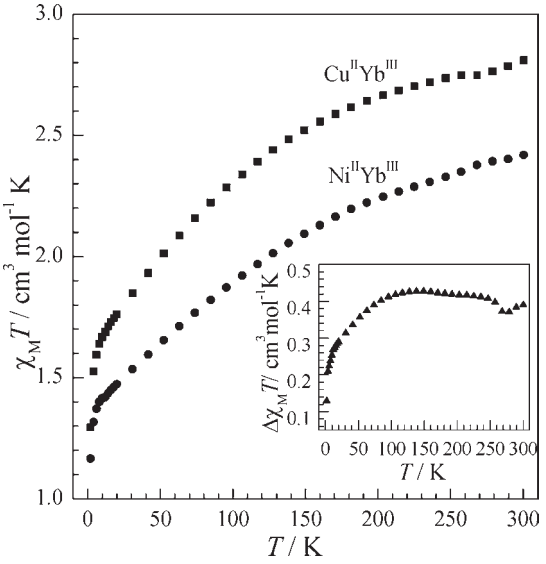

Figure 14. Temperature dependence of blocked $\chi_M T$ for **12** ($Cu^{II}Yb^{III}$) and **24** ($Ni^{II}Yb^{III}$). $\Delta\chi_M T$ versus T profile is shown in the inset.

As shown in Supporting Information, Figures S9−S12 and listed in Table 5, $\Delta\chi_M T$ at 300 K for Pr^{III}, Nd^{III}, Sm^{III}, and Eu^{III} is in the range 0.35−0.50, not very different from the value (0.38) expected for an isolated spin system. $\Delta\chi_M T$ for Eu^{III} is constant throughout the temperature range, indicating no interaction between Cu^{II} and Eu^{III}. It is not surprising to have no exchange interaction between Cu^{II} and Eu^{III} because Eu^{III} has a non-magnetic ground state. In the case of Nd^{III}, the $\Delta\chi_M T$ decreases slowly from 0.41 to 0.34 in the temperature range 300−40 K. $\Delta\chi_M T$ for Sm^{III} is characterized by slow decrease of $\Delta\chi_M T$ from 0.50 to 0.36 on cooling from 300 to 30 K. However, on further cooling from 40 and 30 K for Nd^{III} and Sm^{III}, respectively, $\Delta\chi_M T$ decreases rapidly, indicating antiferromagnetic interaction in both the $Cu^{II}Nd^{III}$ and the $Cu^{II}Sm^{III}$ complexes. For Pr^{III}, $\Delta\chi_M T$ decreases gradually from 0.35 to −0.02 in the temperature range 300−20 K. On further cooling, $\Delta\chi_M T$ increases rapidly. While the rapid increase in the low temperature region may be associated with some intermolecular effect, it can be concluded that the interaction in the $Cu^{II}Pr^{III}$ complex is antiferromagnetic because of the smooth and gradual decrease of the blocked $\Delta\chi_M T$ in most of the temperature range, 300−20 K.

$\chi_M T/\Delta\chi_M T$ versus T Profiles of the $Cu^{II}Gd^{III}$ (6) and $Ni^{II}Gd^{III}$ (18) Complexes. The unblocked $\chi_M T$ of the $Cu^{II}Gd^{III}$ (**6**) compound increases from 8.51 at 300 K to 10.31 at 10−2 K (Supporting Information, Figure S13) because of ferromagnetic interaction between the metal centers.[8a] For the $Ni^{II}Gd^{III}$ (**18**) compound, the unblocked $\chi_M T$ value (7.82) at 300 K is not only almost equal to the theoretical value (7.88) of only gadolinium(III) ion but also remains constant in the temperature range 300−10 K, indicating that the nickel(II) center is diamagnetic and therefore the paramagnetic nature of all the $Ni^{II}Ln^{III}$ complexes **13**−**24** arises because of the lanthanide(III) center. The $\Delta\chi_M T$ value for the $Cu^{II}Gd^{III}$ and $Ni^{II}Gd^{III}$ pair at 300 K is 0.70, greater than that (0.38)

Table 5. $\chi_M T$ and $\Delta\chi_M T$ Values, Observed at 300 K and Theoretical for Isolated Spin Combinations, of **1**−**3**, **4A**, and **5**−**24**

	$\chi_M T$ of $Cu^{II}Ln^{III}$		$\chi_M T$ of $Ni^{II}Ln^{III}$		$\Delta\chi_M T$	
Ln^{III}	observed at 300 K	theoretical[c]	observed at 300 K	theoretical[c]	observed at 300 K	theoretical[c]
Ce[a]	1.14	1.18	0.67	0.80	0.46	0.38
Pr[a]	1.84	1.78	1.49	1.60	0.35	0.38
Nd[a]	1.85	1.79	1.43	1.64	0.41	0.38
Sm[b]	0.94	0.65	0.44	0.32	0.50	0.38
Eu[b]	1.97	1.84	1.49	1.63	0.47	0.38
Gd[b]	8.51	8.25	7.82	7.88	0.70	0.38
Tb[a]	11.70	12.18	11.05	11.81	0.65	0.38
Dy[a]	14.25	14.50	13.87	14.12	0.38	0.38
Ho[a]	14.20	14.42	12.55	14.04	1.65	0.38
Er[b]	11.87	11.82	11.42	11.45	0.46	0.38
Tm[a]	7.28	7.65	6.82	7.28	0.46	0.38
Yb[a]	2.81	2.90	2.42	2.53	0.39	0.38

[a] Blocked data. [b] Unblocked data. [c] For uncorrelated spin combination.

expected for isolated spin combination. Again, increase of $\Delta\chi_M T$ on lowering of temperature (Supporting Information, Figure S13) is in line with the ferromagnetic interaction.[15]

$\chi_M T/\Delta\chi_M T$ versus T Profiles of the $Cu^{II}Ln^{III}$ and $Ni^{II}Ln^{III}$ Complexes (Ln = Dy, Ho, Tm; 8, 9, 11, 20, 21, and 23). For all of the $Cu^{II}Dy^{III}$, $Ni^{II}Dy^{III}$, $Cu^{II}Ho^{III}$, $Ni^{II}Ho^{III}$, $Cu^{II}Tm^{III}$, and $Ni^{II}Tm^{III}$ complexes, blocked $\chi_M T$ decreases slowly from 300 K to a particular lower temperature (60−30 K) and then decreases rapidly (Figure 10 for Dy^{III}, Figure 11 for Ho^{III}, Figure 12 for Tm^{III}). Except for a slight decrease in the higher temperature region for Dy^{III}, $\Delta\chi_M T$ versus T profiles for all these three cases can be considered as similar; the profiles are characterized by gradual increase of $\Delta\chi_M T$ in the temperature range from 300 K to a particular lower temperature followed by rapid decrease on further cooling. Clearly, all these three complexes exhibit intramolecular ferromagnetic interaction, the low temperature decrease may be associated with zero-field effect or intermolecular interaction. As listed in Table 5, $\chi_M T$, 12.55, of the $Ni^{II}Ho^{III}$ complex at 300 K is unusually low in comparison to the theoretical value, 14.04, expected for a Ho^{III} complex. Eventually, although $\chi_M T$, 14.20, of the Cu^{II}-Ho^{III} complex at 300 K is very close to the theoretical value, 14.42, expected for uncorrelated spin combination, $\Delta\chi_M T$, 1.65, at 300 K is significantly higher than 0.38. It is difficult to understand the origin of significant smaller $\chi_M T$ value of the $Ni^{II}Ho^{III}$ complex resulting in a significant larger $\Delta\chi_M T$ value at 300 K of the blocked samples. It may be noted that the unblocked $\Delta\chi_M T$ at 300 K is also almost same, 1.67.

$\chi_M T/\Delta\chi_M T$ versus T Profiles of the $Cu^{II}Er^{III}$ (10) and $Ni^{II}Er^{III}$ (22) Complexes. The unblocked $\chi_M T$ versus T profile of $Ni^{II}Er^{III}$ (**22**) complex is characterized by slow decrease up to 30 K followed by rapid decrease up to 2 K (Figure 13). Although $\chi_M T$ of the $Cu^{II}Er^{III}$ (**10**) complex remains almost constant in the temperature range 300−190 K, this compound also exhibits a sharp increase of $\chi_M T$ on lowering of temperature from 190 to 15 K (Figure 13). On further cooling to 2 K, both the complexes exhibit rapid decrease of $\chi_M T$ from the maxima. The $\chi_M T$ values at 300 K for both the $Cu^{II}Er^{III}$ (observed 11.87, theoretical 11.82) and the $Ni^{II}Er^{III}$ (observed 11.42, theoretical 11.45) complexes are almost identical to the theoretical values expected for noncorrelated spin combinations (Table 5). Eventually, $\Delta\chi_M T$ (0.46) at 300 K for Er^{III}, Figure 13 and Table 5, is almost equal to the theoretical value for the noninteracting situation. Although $\Delta\chi_M T$ remains almost constant down to190 K, an increase of $\Delta\chi_M T$ in the temperature range 190−8 K indicates that Cu^{II} and Er^{III} in the $Cu^{II}Er^{III}$ complex are coupled ferromagnetically.

$\chi_M T/\Delta\chi_M T$ versus T Profiles of the $Cu^{II}Yb^{III}$ (12) and $Ni^{II}Yb^{III}$ (24) Complexes. As shown in Figure 14, the $\chi_M T$ of blocked samples decreases gradually on cooling throughout the temperature range. The $\Delta\chi_M T$ of the Yb^{III} complexes, Figure 14, remains constant in the temperature range 300−70 K but decreases gradually in the temperature range 70−2 K, indicating antiferromagnetic interaction between copper(II) and ytterbium(III).

Comparison of the Exchange Interactions in the Title Compounds with Those of the Previously Reported Systems. Previously, empirical approach has been utilized to understand the nature of interaction in a few series of systems, namely, two diphenoxo-bridged dinuclear Cu^{II}-Ln^{III} series,[14,15] one oxamato-bridged two-dimensional $Cu^{II}Ln^{III}$ series,[11] one cyano-bridged $Fe^{III}Ln^{III}$ series,[13] and one Ln^{III}-radical series.[12] The nature of the exchange interaction in these series of complexes as well as those observed in the present investigation are summarized in Table 6. For the systems involving $4f^{7-13}$ lanthanides in all these series, it is evident that although the interaction is ferromagnetic in most cases, the paramagnetic centers in some cases are noninteracting and even coupled antiferromagnetically. Antiferromagnetic interaction in gadolinium(III) containing complexes in some other systems is also known.[9] Clearly, in contrary to the Kahn's proposition, $4f^{7-13}$ lanthanides may be involved in exhibiting antiferromagnetic coupling. However, in line with the Kahn's proposition, the paramagnetic centers in reported systems involving $4f^{1-6}$ lanthanides are either noninteracting or coupled antiferromagnetically.

It is more relevant to compare the nature of the exchange interaction in the $Cu^{II}Ln^{III}$ complexes in the present investigation, derived from H_2L, with those of the two similar diphenoxo-bridged series, derived from H_2L^1 and H_2L^2. The Ce^{III}, Nd^{III}, and Sm^{III} complexes in all the three series are antiferromagnetically coupled, while there is no interaction in all the three $Cu^{II}Eu^{III}$ complexes. Interestingly, while the two $Cu^{II}Pr^{III}$ complexes derived from H_2L^1 and H_2L^2 are noninteracting, the $Cu^{II}Pr^{III}$

Table 6. Nature of the Magnetic Exchange Interactions in Different Types of Exchange-Coupled Systems Containing Lanthanides as one of the Spin Careers[a]

types of compounds	Ce	Pr	Nd	Sm	Eu	Gd	Tb	Dy	Ho	Er	Tm	Yb
diphenoxo-bridged $Cu^{II}Ln^{III}$ [b]	AF	NI	AF	AF	NI	F	F	F	F	F	AF	AF
diphenoxo-bridged $Cu^{II}Ln^{III}$ [c]	AF	NI	AF	AF	NI	F	F	F	F	?	F	F
diphenoxo-bridged $Cu^{II}Ln^{III}$ [d]	AF	AF	AF	AF	NI	F	F	F	F	F	F	AF
oxamato-bridged 2-D $Cu^{II}Ln^{III}$ [e]	AF	AF	AF	AF		F	F	F	AF	AF	?	AF
cyanobridged $Fe^{III}Ln^{III}$ [f]	AF	NI	AF	NI	NI	AF	F	AF	F	NI	F	NI
radical complex, $R-Ln^{III}-R$ [g]	AF	AF	AF	AF	?	F	F	F	F			

[a] F: ferromagnetic. AF: antiferromagnetic. NI: no interaction. [b] Ref 14. [c] Ref 15. [d] This work. [e] Ref 11. [f] Ref 13. [g] Ref 12.

complex in the present investigation exhibits antiferromagnetic interaction. Regarding the higher analogues, the Gd^{III}, Tb^{III}, Dy^{III}, and Ho^{III} complexes in all the three series are ferromagnetic. The Er^{III} complex in the present investigation and that derived from H_2L^2 exhibit ferromagnetic interaction, while no conclusion could be drawn on the Er^{III} complex derived from H_2L^1. Again, in contrast to the antiferromagnetic interaction in the Tm^{III} and Yb^{III} complexes derived from H_2L^2, the similar two complexes derived from H_2L^1 are ferromagnetically coupled. Clearly, in the highest two analogues, $Cu^{II}Tm^{III}$ and $Cu^{II}Yb^{III}$, the nature of interaction observed in the H_2L^1 and H_2L^2 series are opposite. On the other hand, regarding the interaction in these two analogues in the present investigation, one ($Cu^{II}Tm^{III}$) exhibits ferromagnetic interaction and the second ($Cu^{II}Yb^{III}$) exhibits antiferromagnetic interaction.

The role of the dihedral angle (δ) between the CuO_2 and LnO_2 planes in governing the extent of magnetic exchange interaction in diphenoxo-bridged $Cu^{II}Ln^{III}$ compounds has been already mentioned. The δ values in the compounds derived from H_2L^1 and H_2L^2 are about 4° and 13.5°, respectively, while the ranges of δ values in the present series are 0.8−6.2° in the $4f^{1-7}$ analogues and 17.6−19.1° in the $4f^{8-13}$ analogues. However, since the strength of exchange interaction in the $Cu^{II}Ln^{III}$ compounds derived from H_2L^1 was concluded on the basis of unblocked data and the magnetic field of data collection in the $Cu^{II}Ln^{III}$ compounds derived from H_2L^2 were not mentioned, no meaningful discussion of the strength of magnetic exchange interactions among the compounds of these series is possible.

Conclusions

In the present investigation four types of composition are observed for $Cu^{II}Ln^{III}$ complexes, whereas the $Ni^{II}Ln^{III}$ complexes are characterized with two types of composition. Although some of the $Cu^{II}Ln^{III}$ and $Ni^{II}Ln^{III}$ pairs, with the same lanthanide, have been characterized as isostructural, some other pairs are not. However, the metrical parameters in the coordination environment of the lanthanide(III) center in the two complexes for a pair are not very different, and, more importantly, the lanthanide(III) ion in both the exchange-coupled compound and its reference compound is coordinated by an exactly identical set of atoms. As evidenced from the dihedral angle (δ) between the $CuO(phenoxo)_2$ and $LnO(phenoxo)_2$ planes, a slight variation in the extent of planarity of the bridging moiety in the $Cu^{II}Ln^{III}$ compounds takes place. The bridging moiety in early analogues (Ce−Gd) is almost planar or slightly twisted, whereas that in the latter analogues (Tb−Yb) is significantly twisted. The nature of the magnetic exchange interaction in the $Cu^{II}Ln^{III}$ complexes has been understood by utilizing the empirical approach; the $Ni^{II}Ln^{III}$ complexes have been used as references. The metal centers in the $Cu^{II}Tb^{III}$ (**7**), $Cu^{II}Dy^{III}$ (**8**), $Cu^{II}Ho^{III}$ (**9**), $Cu^{II}Er^{III}$ (**10**), and $Cu^{II}Tm^{III}$ (**11**) complexes are coupled by ferromagnetic interaction, while the $Cu^{II}Yb^{III}$ (**12**) complex exhibits antiferromagnetic interaction. On the other hand, among the lower members of the series, $Cu^{II}Ce^{III}$ (**1**), $Cu^{II}Pr^{III}$ (**2**), $Cu^{II}Nd^{III}$ (**3**), and $Cu^{II}Sm^{III}$ (**4A**) exhibit antiferromagnetic interaction, whereas the $Cu^{II}Eu^{III}$ (**5**) complex behaves as a spin-uncorrelated system.

The magnetic properties in the present investigation have been compared with those of the other reported series, two similar diphenoxo-bridged series in particular. In contrast to the previously reported noninteracting diphenoxo-bridged $Cu^{II}Pr^{III}$ systems, it is interesting that the $Cu^{II}Pr^{III}$ (**2**) compound exhibits antiferromagnetic interaction. Again, the magnetic exchange interaction in the three $Cu^{II}Tm^{III}$ and three $Cu^{II}Yb^{III}$ complexes in the three series are not matched with each other, indicating the difficulty of prediction of magnetic properties of lanthanide containing exchange-coupled compounds. More such series should be explored to frame better structure-property correlations.

An important aspect of the present study is the measurement of the magnetic susceptibility of the unblocked samples as well as on blocking the samples with grease to avoid powder reorientation, if any. Comparison of the unblocked and blocked data reveals significant difference in some cases. For example, the $Cu^{II}Ce^{III}$ complex exhibits ferromagnetic interaction on the basis of unblocked data but antiferromagnetic interaction on the basis of blocked data. Again, the nature of interaction in the $Cu^{II}Tb^{III}$, $Cu^{II}Dy^{III}$, and Cu^{II}-Yb^{III} compounds can not be concluded from the unblocked data, but the nature of the interaction in these three compounds can be well understood on blocking the samples with grease. It seems therefore that the magnetic measurement of the lanthanide containing compounds should be carried out or checked on blocking the samples with grease. The conclusion regarding the nature and strength of the magnetic exchange interaction in the lanthanide containing complexes may be changed if the measurements would be carried out on blocking the samples with grease. Clearly, this area deserves more attention and should be explored more.

Acknowledgment. Financial support from the Department of Science and Technology, the Government of India (SR/S1/IC-12/2008), Council for Scientific and Industrial Research (Fellowship to A.J. and S.M.), and Centre for Research in Nanoscience and Nanotechnology (Fellowship to R.K.) are gratefully acknowledged. Single crystal X-ray crystallographic studies of **2**, **16**, and **18** have been carried out at the DST (Government of India)−FIST funded Single Crystal X-ray Diffractometer

Facility at the Department of Chemistry, University of Calcutta.

Supporting Information Available: Crystallographic data in CIF format for the compounds **1**−**4**, **7**, **9**, **10**, **12**, **13**, **16**, **18**, and [$Ni^{II}L\subset(H_2O)$], Tables S1−S8, Figures S1−S13, discussion on the utilization of empirical approach to understand the nature of magnetic exchange interaction in the title compounds, and characterization as well as determination and description of the crystal structure of [$Ni^{II}L\subset(H_2O)$]. This material is available free of charge via the Internet at http://pubs.acs.org.